Clays and Clay Minerals, Vol. 60, No. 6, 633–654, 2012.

MINERALOGY AND GEOCHEMISTRY OF THE SEDIMENTARY KAOLIN DEPOSITS FROM SINAI, EGYPT: IMPLICATIONS FOR CONTROL BY THE SOURCE ROCKS

HASSAN M. BAIOUMY[1,*], H. ALBERT GILG[2], AND HEINRICH TAUBALD[3]

[1] Central Metallurgical R & D Institute, PO Box 87 Helwan, Cairo, Egypt
[2] Lehrstuhl für Ingenieurgeologie, Technische Universität München, 80290, München, Germany
[3] Lehrstuhl für Isotopengeochemie, Universität Tübingen, 72074 Tübingen, Germany

Abstract—Mineralogical and geochemical variations among the Carboniferous and Cretaceous sedimentary kaolin deposits from Sinai provided an opportunity to examine the effect of the source area on compositions of the deposits. The Carboniferous kaolin deposits are mineralogically and geochemically heterogeneous. The Khaboba and Hasbar deposits consist of kaolinite, quartz, anatase, illite, chlorite, zircon, and leucoxene. The shale-normalized rare earth element (*REE*) patterns of the Khaboba deposit showed a slight *LREE* over *HREE* enrichment ($(La/Yb)_{SN}$ = 1.19−1.51) with a *MREE* depletion (Gd/Gd^*_{SN} = 0.51−0.75), while the Hasbar kaolin had a *MREE* enrichment. The Abu Natash kaolin deposit consisted of kaolinite, anatase, and a little quartz with larger TiO_2, Cr, and V and smaller Zr and Nb contents compared to other Carboniferous deposits. The shale-normalized *REE* patterns of the Abu Natash deposit exhibited a positive Eu anomaly (Eu/Eu^*_{SN} = 1.28−1.40) and a *MREE* enrichment (Gd/Gd^*_{SN} = 1.41−2.05). The Cretaceous deposits were relatively homogeneous in terms of mineralogical composition and geochemistry and are composed of kaolinite, quartz, anatase, rutile, zircon, and leucoxene. The Cretaceous kaolin deposits showed mostly flat shale-normalized *REE* patterns with a variable *LREE* depletion.

The presence of illite and chlorite, the absence of rutile, large Zr and Nb contents, and the *REE* patterns suggested a component of weathered low-grade metasediments as a source for the Carboniferous deposits in the Khaboba and Hasbar areas, while the large Ti, Cr, and V, and small quartz contents indicated mafic source rocks for the Abu Natash deposit. The abundance of high-Cr rutile and the absence of illite and chlorite, and large Zr, Ti, Cr, and V contents suggested a mixture of medium- to high-grade metamafic and granitic rocks as source rocks for the Cretaceous kaolin deposits. The occurrence of alkaline rocks in the source of the deposits studied was identified by high-Nb contents and the presence of bastnaesite. The mineralogical and geochemical heterogeneity and lesser maturity of the Carboniferous deposits suggested local sources for each deposit and their deposition in basins close to the sources. The mineralogical and geochemical homogeneity and maturity of the Cretaceous deposits, on the other hand, indicated common sources for all deposits and their deposition in relatively remote basins.

Key Words—Egypt, Geochemistry, Mineralogy, Origin, Sedimentary Kaolin Deposits, Sinai, Source.

INTRODUCTION

Kaolin deposits are developed in a wide range of kaolinite-bearing lithologies and generally classified into primary kaolin deposits formed by *in situ* alteration of igneous or metamorphic protoliths, and secondary, sedimentary kaolin deposits that involve sedimentary, clay-rich rocks (*e.g.* Murray and Keller, 1993; Pruett and Pickering, 2006; Murray, 2007). The latter type, in particular, such as the Georgia (USA) and Capim River (Brazil) kaolin deposits, represent the current, and probably future, major supplies of kaolin to world markets (*e.g.* Costa and Moraes, 1998; Pruett and Pickering, 2006) and may be of strategic interest also for developing countries (Knill, 1978). Sedimentary kaolin deposits often have a complex geological history with one or more superimposed alteration processes (*e.g.* Hurst and Pickering 1997; Pruett and Pickering, 2006; Baioumy and Gilg, 2011). Nevertheless, their mineralogical and geochemical characteristics reflect, in large part, the weathering processes in lithologically specific source regions and mineral sorting during transport and deposition (*e.g.* Dombrowski and Murray, 1984; Pruett and Murray, 1993; Baioumy and Gilg, 2011). Sedimentary kaolin deposits can, therefore, be considered as geological-geochemical archives of once-eroded source regions that include significant paleoclimatic information. Post-depositional alteration may modify some of the mineralogical-geochemical properties (*e.g.* Hurst and Pickering 1997; Schroeder *et al.*, 2004). All of these geological processes together exert significant influence on kaolin quality and utilization (*e.g.* Elzea Kogel *et al.*, 2002; Murray, 2007) and, therefore, merit study.

The sedimentary kaolin deposits of the Sinai Peninsula, Egypt (Figure 1), with reserves of >100 Mt are of major economic importance in northern Africa. Currently ~100,000 t of kaolin are exploited each year mostly for domestic uses, including refractories, ceramics,

* E-mail address of corresponding author:
hassanbaioumy@hotmail.com
DOI: 10.1346/CCMN.2012.0600608

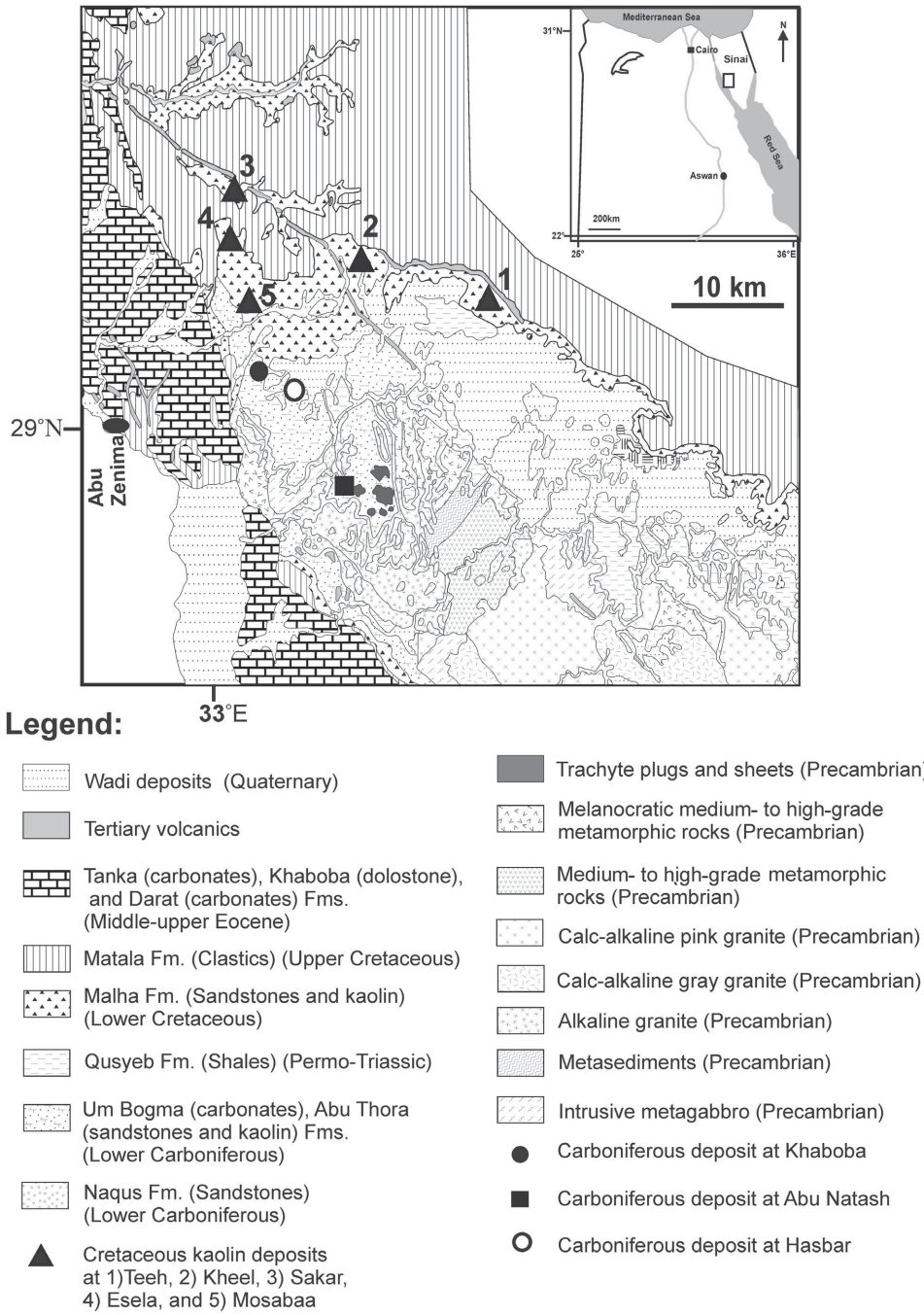

Figure 1. Geological map of the Sinai Peninsula showing the locations of the Carboniferous and Cretaceous sedimentary kaolin deposits as well as the Precambrian igneous and metamorphic basement rocks. The map was adapted from a geological map of Egypt published by the Geological Survey of Egypt.

and white-concrete industries. Despite their economic significance, a few studies, mostly mineralogical and radiometric, have focused on these deposits (*e.g.* Rashed and Amer, 1994; Boulis and Attia, 2001; Walley El-Dine *et al.*, 2004; El-Shishtawy *et al.*, 2006, 2008).

The kaolin deposits were deposited during the Carboniferous and Cretaceous at the northwestern rim of the Arabian Nubian Shield (ANS) and, thus, represent a unique 200 million year archive for weathering of the uplifted juvenile Panafrican shield. In the present study, the mineralogical and chemical compositions of the Sinai kaolin deposits from both epochs were characterized and compared in order to investigate the control on sedimentary kaolin composition and quality exerted by

source rocks from different erosional levels of the ANS. Unlike many previous studies which investigated bulk compositions exclusively, the present study gathered comprehensive mineralogical and geochemical data on the bulk samples, sand fractions, and clay fractions of the kaolin deposits.

GEOLOGICAL SETTING

The Carboniferous sedimentary rocks in west-central Sinai comprise the Um Bogma and Abu Thora Formations (Figure 2A). The Um Bogma Formation consists of a lower and upper sandy dolostone unit separated by the argillaceous and dolomitic limestone unit characterized by thin laminated siltstone and shale intercalations (Kora *et al.*, 1994). The Um Bogma Formation hosts important hydrothermal ferromanganese deposits that replaced the upper sandy dolostone unit. The overlying Abu Thora Formation (30–200 m) is composed mainly of siliciclastic sandstones and includes rare white glass sands and the Carboniferous kaolin deposits (Weissbrod, 1969).

The Carboniferous sedimentary kaolin deposits are located in the Khaboba and Hasbar areas between the latitudes 29º03′00′′ and 29º13′30′′N and longitudes 33º10′00 and 33º16′33′′E north and east of Abu Zenima, west-central Sinai (Figure 1). The kaolin deposit in the Khaboba area (Figure 2B) occurs in the form of lenses that attain a maximum thickness of ~2.5 m of moderately hard, gray to dark gray, massive or rarely laminated kaolin (Figure 3a). The uppermost part of the Khaboba kaolin deposit is yellowish to reddish in color (Figure 3b) due to the presence of Fe oxide that was probably derived from the overlying Fe-rich sandstones. Black to dark gray kaolin beds (Figure 3c) as well as very thin (~10 cm) white to whitish gray and very fine alunite veins occur within the kaolin deposit (Figure 3d). The Hasbar kaolin deposit that occurs as lenses 1–3 m thick (Figure 2C) is harder and darker in color (Figure 3e) compared to the Khaboba kaolin. Carboniferous sedimentary kaolin deposits are also found in the Wadi Abu Natash, El Shellal, and Mukattab areas, southeast of Abu Zenima. The whitish gray to earthy gray, massive, moderately hard kaolin beds of the Abu Natash deposit (Figure 3f) range in thickness from 30 to 180 cm and are intercalated in sandstones (Figure 2D). These kaolin deposits, unlike those of Khaboba and Hasbar, are devoid of alunite veins and organic matter.

The Lower Cretaceous sedimentary sequences in west central Sinai include four formations, namely the Malha, Galala, Halal, and Wata Formations (Figure 4I). The

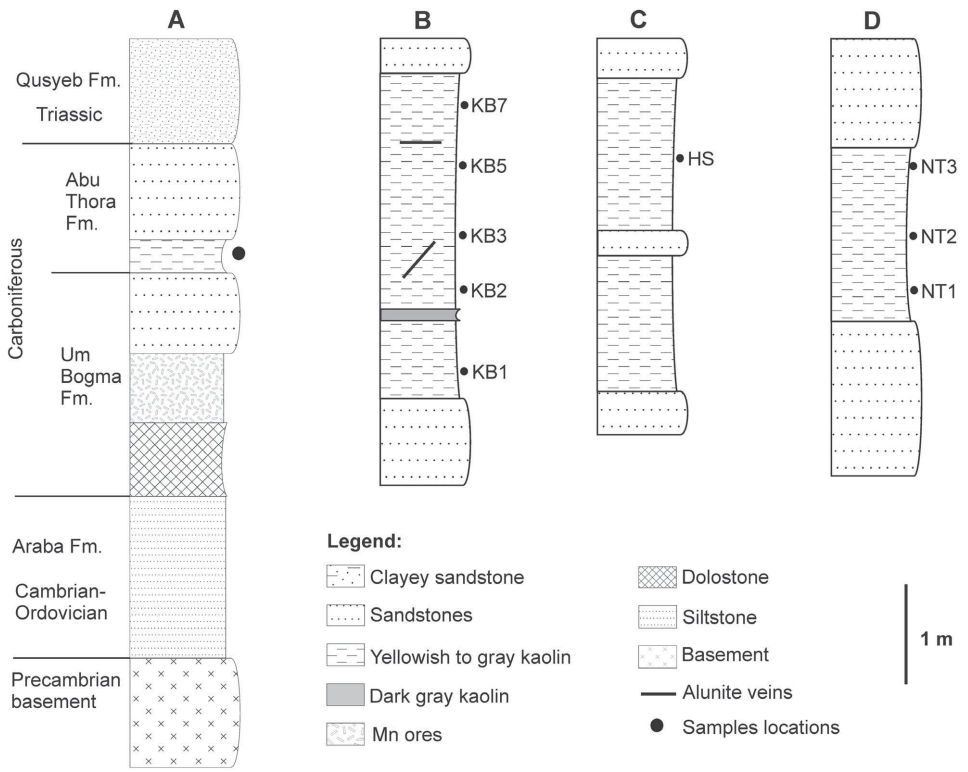

Figure 2. General lithostratigraphy of the Carboniferous sedimentary sequence in the Sinai Peninsula: (A) the stratigraphic position of the Carboniferous kaolin deposits (not to scale); (B, C, and D) measured lithostratigraphic sections of a kaolin deposit at the Khaboba, Hasbar, and Abu Natash areas, respectively.

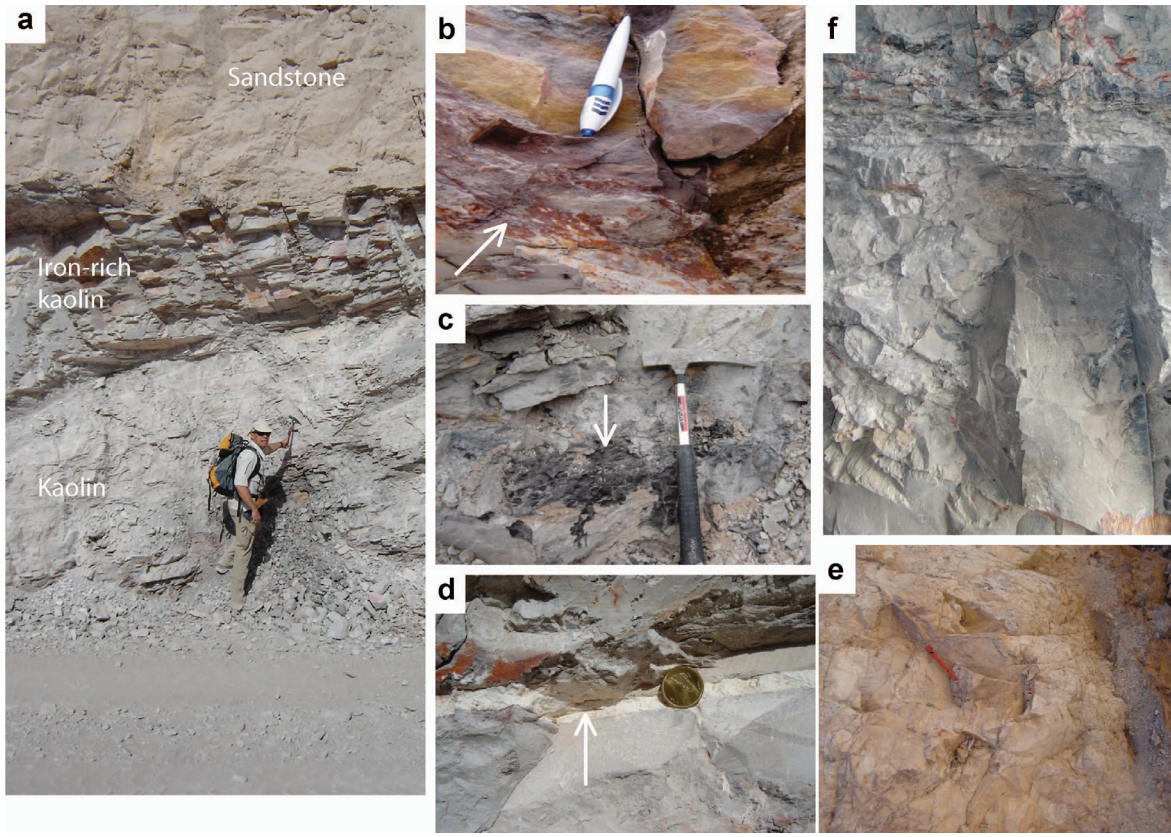

Figure 3. Field photographs of the Carboniferous kaolin deposits from Sinai. (a) General view of the kaolin deposit at the Khaboba area, overlain by sandstone. (b) Fe-rich kaolin at the top of the Khaboba kaolin deposit in contact with the overlying sandstone. (c) Dark gray to black organic-rich beds within the Khaboba deposit (arrow). (d) Close up to the white alunite veins inside the deposit (arrow). (e) General view of the kaolin deposit in the Hasbar area. (f) Kaolin deposit at the Abu Natash area.

basal Malha Formation that hosts the Cretaceous kaolin deposits in Sinai (Abdallah *et al.*, 1963) consists predominantly of gray, ferruginous, cross-bedded sandstones with a few interbeds of green silty shales and calcareous sandstones (Abu-Zied, 2008). The lower part of the Galala Formation consists of sand bodies intercalated with calcareous mudstones, shale, and thin beds of limestone. The middle and upper parts comprise fossiliferous limestone, dolostone, marls, and mudstones (Aboul Ela *et al.*, 1990). The Halal Formation is composed mainly of grayish white hard dolomitic limestone and dolostones with minor clastic intercalations (Nabawy, 2010). The Wata Formation consists of marls, marly limestone, dolomitic limestone, and nodular limestone (Ghorab, 1961).

The Lower Cretaceous sedimentary kaolin deposits in the Malha Formation in west-central Sinai occur mainly in two areas: (1) north and northeast of Abu Zenima, covering an area of 200 km^2 between latitudes 29º03′00″ and 29º13′30″N and longitudes 33º10′00″ and 33º16′33″E with the Mosabaa, Esela, Hanash, and Teeh deposits; and (2) south of Abu Zenima, covering an area of 150 km^2 between latitudes 28º52′30″ and 28º58′30″N and longitudes 33º13′00″ and 33º23′00″E in the Farsh El-Ghozlan, Dehesa, Wadi Abu Natash, and Wadi Budra areas. The present study focused on the deposits from the Teeh, Esela, and Mosabaa areas as these kaolin deposits have the largest reserves and are presently the most productive mines in the area. The Teeh Plateau is situated ~25 km northeast of Abu Zenima on the asphalt road to Um Bogma. It covers an extensive area separating the northern and southern Sinai. The local measured kaolin resource is ~90 million tons. Three sections were investigated and sampled at the Teeh Plateau, namely, the Teeh, Kheel, and Sakar deposits. In the Teeh section (Figure 4II), kaolin is mined at three levels, A, B, and C. In level A, the kaolin deposit occurs as separated beds that range in thickness from 30 cm to 1.5 m within yellowish to reddish sandstones. The kaolin deposits are massive, sometimes laminated, moderately hard, dark gray, pale gray, and brownish to yellowish gray (Figure 5a). The uppermost part of this level is rich in dark gray to black kaolin deposits that host thin bands (~10 cm thick) of lignite (Figure 5a). Plant remains, including tree branches, occur within the kaolin deposits. Sandstone

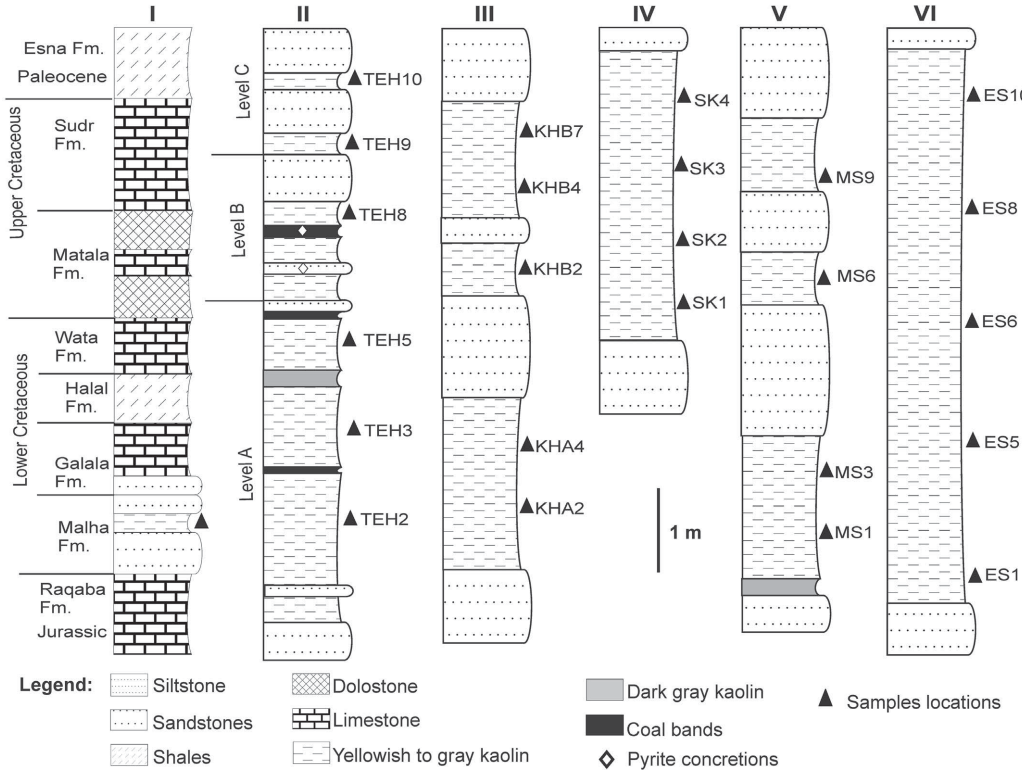

Figure 4. General lithostratigraphic section of the Cretaceous sedimentary sequence in the Sinai Peninsula. I: the stratigraphic position of the Cretaceous kaolin deposits (not to scale). II, III, IV, V, and VI: measured lithostratigraphic sections of the kaolin deposit at the Teeh, Kheel, Sakar, Mosabaa, and Esela areas, respectively.

and coals in this part of level A are also particularly rich in large euhedral pyrite crystals (Figure 5b). The kaolin deposits of levels B and C are yellowish gray, faintly laminated, and moderately hard. The kaolin deposits of the Kheel (Figure 4III) and Sakar (Figure 4IV) mines are similarly intercalated in partly ferruginous sandstones. In the Kheel section, the massive, moderately hard, black, dark gray, pale gray, brownish, or yellowish gray kaolin beds range in thickness from 10 cm to 2 m (Figure 5c), while the Sakar kaolin beds attain a much greater thickness of ~4 m (Figure 5d). The kaolin deposit in the Mosabaa area occurs as lenticular beds in three horizons that are separated by sandstones (Figure 4V). The lower horizon consists of a 20 cm-thick dark gray to black, moderately hard, and massive kaolin, rich in plant remains, which is overlain by 1 m of gray, massive, hard kaolin. A hard, massive, reddish, Fe-rich and a very hard, massive, siliceous kaolin bed follows in the stratigraphic sequence (Figure 5e). The second and third horizons host yellowish gray massive, moderately hard kaolin deposits with occasional red hematite staining. The variably colored kaolin deposits of the Esela mine attain a maximum thickness of ~7 m (Figure 4VI). Again, a reddish Fe-oxide staining is observed at the uppermost part of the kaolin bed (Figure 5f).

MATERIALS AND METHODS

Thirty three kaolin samples were collected from different localities in the Carboniferous (nine samples) and Cretaceous (24 samples) deposits in the Sinai Peninsula. The Carboniferous deposits were represented by the Khaboba, Hasbar, and Abu Natash areas, while the Teeh, Kheel, Sakar, Esela, and Mosabaa areas represented the Cretaceous deposits. The samples collected were subjected to detailed mineralogical and geochemical investigations as follows.

Grain-size distributions of a number of these samples were determined by sedimentation from aqueous suspensions after complete disaggregation of the bulk clays. A 10-g sample of the bulk clays was soaked in distilled water for ~2 weeks. During this period, the samples were treated ultrasonically three times (10−15 min each time) using a cleaning ultrasonic instrument (Model BK-1800, Jinan Bakr Ultrasonic Technology Co. Ltd, China) and then washed several times using distilled water until a suspension at pH ranging from 7 to 8 was reached. To avoid any contamination of the clay fractions, no dispersant chemicals were used. Sand fractions (>63 mm) produced from this step were treated with sodium polytungstate heavy liquid at a specific gravity of 2.8 to separate heavy minerals, which were prepared as polished sections afterwards. Forty two rutile grains

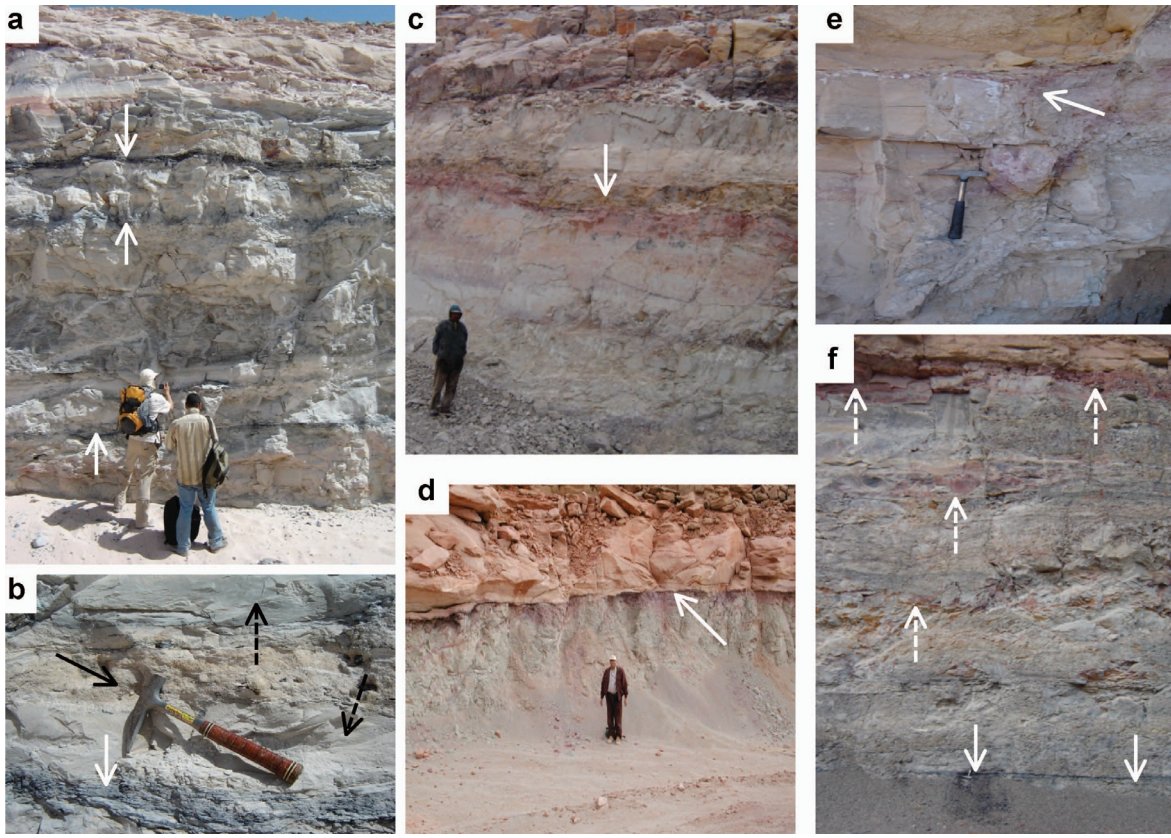

Figure 5. Field photographs of the Cretaceous kaolin deposits from Sinai. (a) General view of the kaolin deposit at the Teeh Plateau with the black and dark gray coal and organic-rich beds (arrows), especially in the upper part of the section. (b) A close-up view to the Teeh deposit showing the intercalations of coal (white arrow) and sandstone (black arrow) with the kaolin beds (dotted arrows). (c) View of the kaolin deposit at the Kheel section with the Fe-rich horizon (arrow) within the deposit. (d) Greenish gray kaolin at the Sakar area with the Fe-rich kaolin (arrow) at the top of the section. (e) Kaolin deposit at the Mosabaa section with the Fe-rich horizon (arrow) at the top of the deposit. (f) General view of the kaolin deposit at the Esela area with the organic-rich beds in the lower part of the photo (solid arrows) and Fe-rich parts (dotted arrows), especially at the top of the section.

from the kaolin deposits were analyzed for their chemical compositions using laser ablation inductively coupled plasma mass spectrometry (LA-ICP-MS) at Erlangen University, Germany (Merchantek 266 LUV laser coupled to an Agilent 7500i ICP-MS with an Ar carrier gas). NIST 612 50 ppm glass was used for external calibration. Representative kaolin samples were observed with a LEO 1530 VP Gemini field-emission scanning electron microscope (FE-SEM) at the Centre for Material Analysis (ZWL), Lauf, Germany. The clay fractions (<2 μm) were separated from the same aqueous suspensions after ~7 h to ensure their purity. The clay fractions were precipitated on glass slides to investigate the clay mineralogy of the deposits studied. Both bulk and clay fractions (air-dried, glycolated, and heated at 550ºC) were analyzed for their mineralogical composition by X-ray diffraction (XRD) using a Philips PW1800 instrument (CuKα radiation, 40 kV, 40 mA). The quantitative mineralogical compositions were determined using the Rietveld program BGMN® (Kleeberg and Bergmann, 1998) and chemical composition. The degree of structural disorder of the kaolin studied was evaluated using the Hinckley Index (HI) (Hinckley, 1963; Galán *et al.*, 1994) of the clay fractions (<2 μm). The chemical composition for major and trace elements of the bulk deposits and clay fractions were determined on fused Li tetraborate beads using a Bruker AXS S4 Pioneer X-ray fluorescence (XRF) analyzer with a Rh anode (40−60 kV, 40−45 mA) at Tübingen University, Germany.

The *REE* concentrations of the clay fractions were determined using a Perkin-Elmer/SCIEX ELAN 5000 ICP-MS at the Helmholtz-Zentrum Potsdam Deutsches GeoForschungsZentrum (GFZ), Potsdam, Germany. 0.1 g of each clay fraction sample was reacted for 6 h with 1 mL of 1 N HCl prior to dissolution to release adsorbed and easily exchangeable elements. The residues were digested with 2 mL of 49% HF in capped teflon bombs on an electric hot plate (~150ºC) for 24 h. The solution was evaporated to near dryness, and redissolved in 2 mL of 6 N HNO_3 in capped teflon bombs at 150ºC for 2 days. The samples were then evaporated

to near dryness, 1 mL of 6N HNO_3 was added, and the solutions were further diluted for analysis.

RESULTS

Grain-size analysis

The grain-size distributions (Tables 1 and 3) revealed larger silt contents in the Carboniferous deposits (average of 25.1 wt.%) compared to the Cretaceous deposits (average of 8.7 wt.%). Consequently, the Cretaceous kaolin deposits have greater clay fraction contents (average of 89.9 wt.%) than the Carboniferous kaolin deposits (average of 73.3 wt.%). No significant difference was observed in the sand contents of either deposit (averages of 1.7 and 1.4 wt.% for the Carboniferous and Cretaceous deposits, respectively).

Table 1. Grain-size distribution (wt.%), mineralogical compositions (wt.%), geochemistry of major oxides (wt.%), and trace elements (ppm) and alteration indices of the bulk samples of the Carboniferous kaolin deposits, Sinai.

Sample	KB1	KB2	KB3	KB5	KB7	HS	NT1	NT2	NT3
Sand	1.4	0.8	1.6	4.1	0.4				
Silt	20.1	24.5	28.9	24.9	27.2				
Clay	78.5	74.8	69.5	71.0	72.5				
Kaolinite	70	65	59	60	63	37	95	96	95
Quartz	23	29	33	32	30	55	T	nd	1
Anatase	1	1	1	2	2	1	4	3	3
Alunite	1	1	5	3	2	3	nd	nd	nd
Hematite	1	2	nd	nd	nd	nd	nd	nd	T
Illite	2	1	1	2	2	3	nd	nd	nd
Microcline	T	T	T	T	T	T	T	T	T
SiO_2	52.03	57.08	58.32	61.50	60.74	72.14	42.90	43.42	43.12
TiO_2	1.47	1.41	1.47	1.50	1.58	1.40	4.11	2.91	2.72
Al_2O_3	23.22	24.84	24.59	25.44	26.18	15.14	37.05	37.76	37.41
Fe_2O_3*	2.80	4.07	0.74	0.87	0.72	0.50	0.87	0.76	1.68
MnO	bdl	bdl	bdl	bdl	bdl	bdl	bdl	bdl	bdl
MgO	0.34	0.28	0.31	0.39	0.36	0.33	0.34	0.24	0.28
CaO	0.14	0.13	0.05	0.08	0.08	0.31	0.06	0.08	0.25
Na_2O	0.40	0.24	0.31	0.18	0.17	0.28	0.09	0.10	0.14
K_2O	0.71	0.79	1.46	0.86	0.78	0.80	0.03	0.02	0.01
P_2O_5	0.06	0.06	0.07	0.07	0.06	0.14	0.16	0.15	0.13
LOI	18.24	11.63	12.87	9.59	9.94	8.14	14.06	13.99	14.03
Sum	99.4	100.5	100.2	100.5	100.6	99.2	99.7	99.4	99.8
Ba	162	186	234	214	187	208	42	52	42
Co	bdl	2	bdl	bdl	bdl	bdl	bdl	bdl	bdl
Cr	90	108	88	92	97	48	274	274	305
Nb	53	53	52	53	58	53	36	36	32
Ni	142	79	69	59	55	47	11	3	10
Rb	34	34	53	46	40	34	bdl	bdl	bdl
Sr	93	139	203	110	93	290	571	517	403
V	218	218	178	144	140	103	349	349	359
Y	48	58	58	56	59	78	26	36	33
Zn	24	6	21	11	bdl	bdl	59	17	29
Zr	394	440	432	385	413	441	188	178	155
CIA	93.8	94.9	92.2	95.5	95.9	90.7	99.5	99.5	99.4
ICV	0.25	0.28	0.18	0.15	0.14	0.24	0.15	0.11	0.14

KB = Khaboba deposit
HS = Hasbar deposit
NT = Abu Natash deposit
T = traces (detected but <0.5 wt.%)
LOI = Loss on ignition
nd = not detected
bdl = below detection limit
* Total iron as Fe_2O_3
CIA: chemical index of alteration
ICV: Index of composition variability

Optical studies

The heavy minerals that were separated from the Carboniferous Khaboba kaolin deposit were dominated by very fine sand-sized leucoxene and traces of ilmenite. Under the reflected light microscope, leucoxene occurred as rounded to subrounded, spherical grains of intermediate metallic luster that gave pale brown to yellowish brown colors under crossed polars and was characterized by a sponge-like texture (Figure 6a). A few ilmenite grains of irregular shape and high metallic luster were identified (Figure 6b). These grains were dark blue in color under plain polars. Rutile, leucoxene, and zircon were the predominant heavy minerals in the sand fraction of the Cretaceous Mosabaa deposit (Figure 6c,d). They all occurred as rounded to subrounded, spherical to elongate grains. Under the reflected light microscope, rutile was characterized by a high reflectance with a reddish brown color under crossed polarized light, while zircon showed rather pale gray colors and low reflectance (Figure 6d).

SEM studies

Under the SEM, kaolinite from the Khaboba and Hasbar deposits occurred as crystals of variable size (1–20 mm), mostly with undefined outlines and edges and rarely as kaolinite pseudomorphs after biotite (stacks of book-like shape) (Figure 7a). Silt-size quartz was quite common in both deposits. Mica plates of relatively coarse grain size (Figure 5b) and cubes of fine-grained alunite (Figure 7c) were identified in the Hasbar deposit. In addition, several accessory minerals such as galena (Figure 7d), monazite (Figure 7e), and aluminum phosphate minerals (Figure 7f) in the silt-size material were identified in the Khaboba deposit, based on their chemical compositions using the EDX technique. Under the SEM, kaolinite from the Teeh deposit occurred as anhedral flakes ranging from <1 μm to 20 μm in diameter (Figure 7g). Zircon grains showed cracks and internal zoning sometimes with inclusion of an F- and *REE*-rich carbonate mineral, probably bastnaesite (Figure 7h).

XRD studies

The results of quantitative mineralogical analyses of bulk samples from the Carboniferous kaolin deposits (Table 1) showed that the Abu Natash deposit has a different mineralogical composition from the Khaboba and Hasbar deposits (Figures 8a). The Abu Natash kaolin has more kaolinite (~ 95 wt.%) and anatase (~3 wt.%) and smaller quartz (~1 wt.%) contents than the Khaboba and Hasbar deposits. In addition, no alunite or illite were identified in the Abu Natash deposit. The Hasbar deposit contains less kaolinite (~36 wt.%) and more quartz (~56 wt.%) and illite (~2.5 wt.%) than the Khaboba

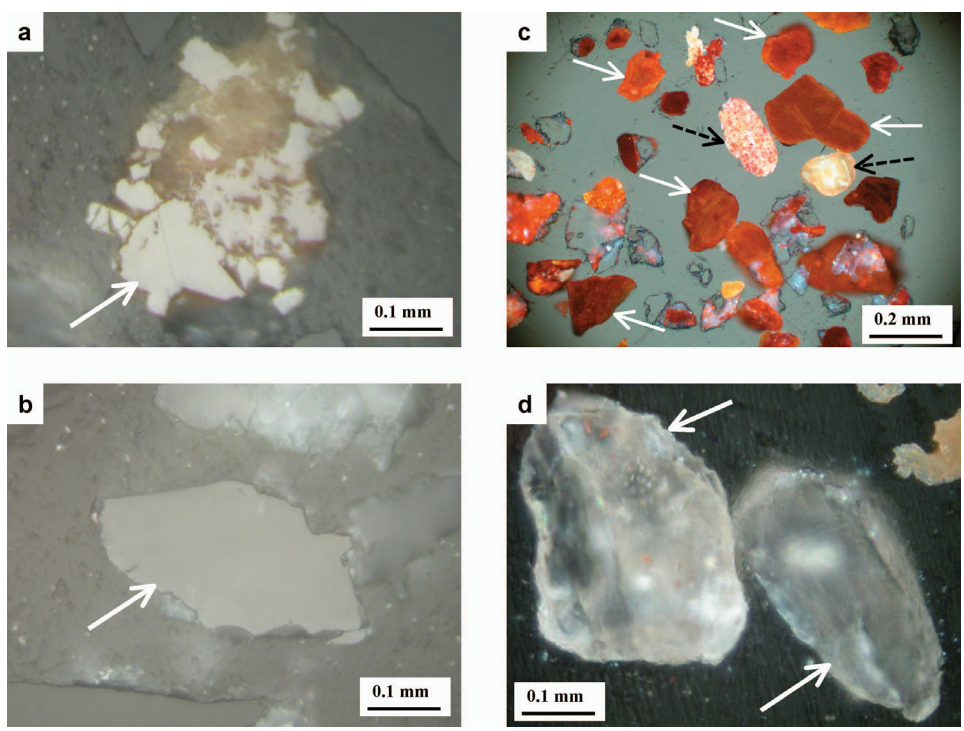

Figure 6. Reflected light photomicrographs of heavy minerals in the Carboniferous and Cretaceous kaolin deposits from Sinai. (a, b) Leucoxene and ilmenite grains from the Carboniferous deposits, respectively. Arrows indicate the mineral grains. (c) Rutile (solid white arrows) and leucoxene (black dotted arrows). (d) Zircon from the Cretaceous deposits (arrows).

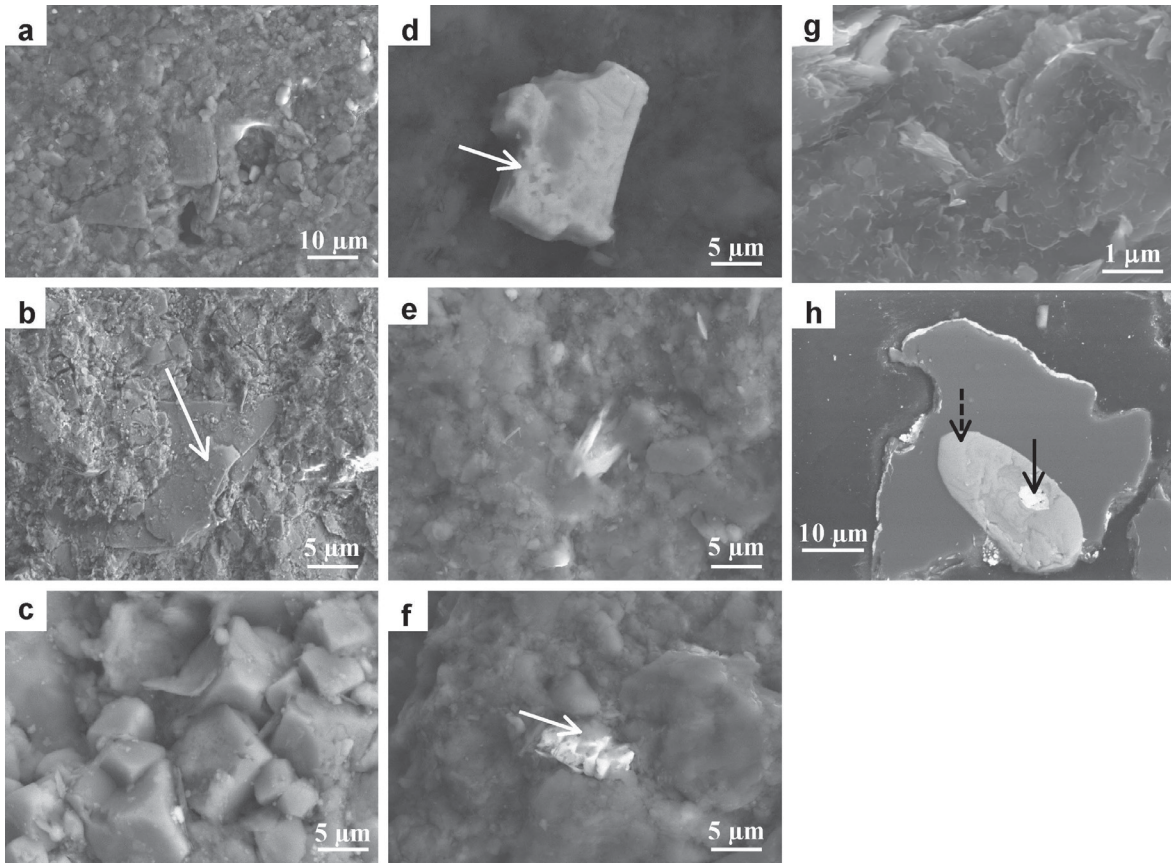

Figure 7. SEM images of the Carboniferous and Cretaceous kaolin deposits from Sinai. (a–f) Kaolinite, illite, alunite cubes, galena, monazite, and aluminum phosphate minerals from the Carboniferous deposits, respectively. Arrows indicate the mineral grains. (g,h) Kaolinite and zircon (dotted arrow) with a bastnaesite inclusion (solid arrow) from the Cretaceous deposits, respectively.

deposit (63, 29, and 1.3 wt.% for kaolinite, quartz, and illite, respectively). With few exceptions, microcline and hematite occurred as traces in all deposits. In the clay fractions (Table 2, Figure 8b), the kaolinite contents were greater in all deposits, especially in the Hasbar deposit, at the expense of quartz contents. Traces of chlorite (1.3–1.6 wt.%) were identified in some samples from the Khaboba deposit. No hematite was detected in the clay fractions of any deposits. Anatase occurs mostly in the very fine fractions, and was particularly enriched in the Abu Natash deposit (Figure 8a,b). Mineralogical analyses of bulk samples and clay fractions of the Cretaceous deposits indicated that kaolinite, quartz, and anatase are the major constituents of all deposits with traces of hematite and microcline (Table 3, Figure 9a). In the bulk samples, the Sakar followed by the Esela deposit contained greater amounts of kaolinite (averages of 88 and 85 wt.%, respectively) and less quartz (averages of 9 and 12 wt.%, respectively) when compared to the Mosabaa, Kheel, and Teeh deposits (kaolinite contents of 65, 76, and 75%, respectively, and quartz contents of 31, 21, and 22 wt.%, respectively). The anatase, microcline, and hematite contents showed no significant differences among the deposits. The anatase contents ranged between 1.2 and 4.2 wt.% with an average of 2.2 wt.%. In the clay fractions (Table 4, Figure 9b), the kaolinite contents were slightly greater in all deposits, at the expense of quartz. Although no significant differences in the mineralogy of the clay fractions among the different Cretaceous deposits were observed, the clay fractions from these kaolin deposits had smaller quartz and greater kaolinite contents (averages of 5.5 and 91%, respectively) compared to the Carboniferous deposits (averages of 10 and 82.6 wt.%, respectively). Values of the Hinckley Index (HI) ranged from 0.60 to 0.85 for the Carboniferous kaolin deposits and from 0.53 to 0.86 for the Cretaceous deposits (Tables 2 and 4, respectively) indicating a medium-order kaolinite of both deposits.

Geochemistry

Major elements. Major-element distributions among the Carboniferous deposits (Tables 1, 2) indicated that the bulk samples of the Hasbar deposit have greater SiO_2 contents (~72 wt.%) than the Khaboba and Abu Natash deposits (averages of 58 and 43 wt.%, respectively) due to their greater quartz contents. The Hasbar deposit

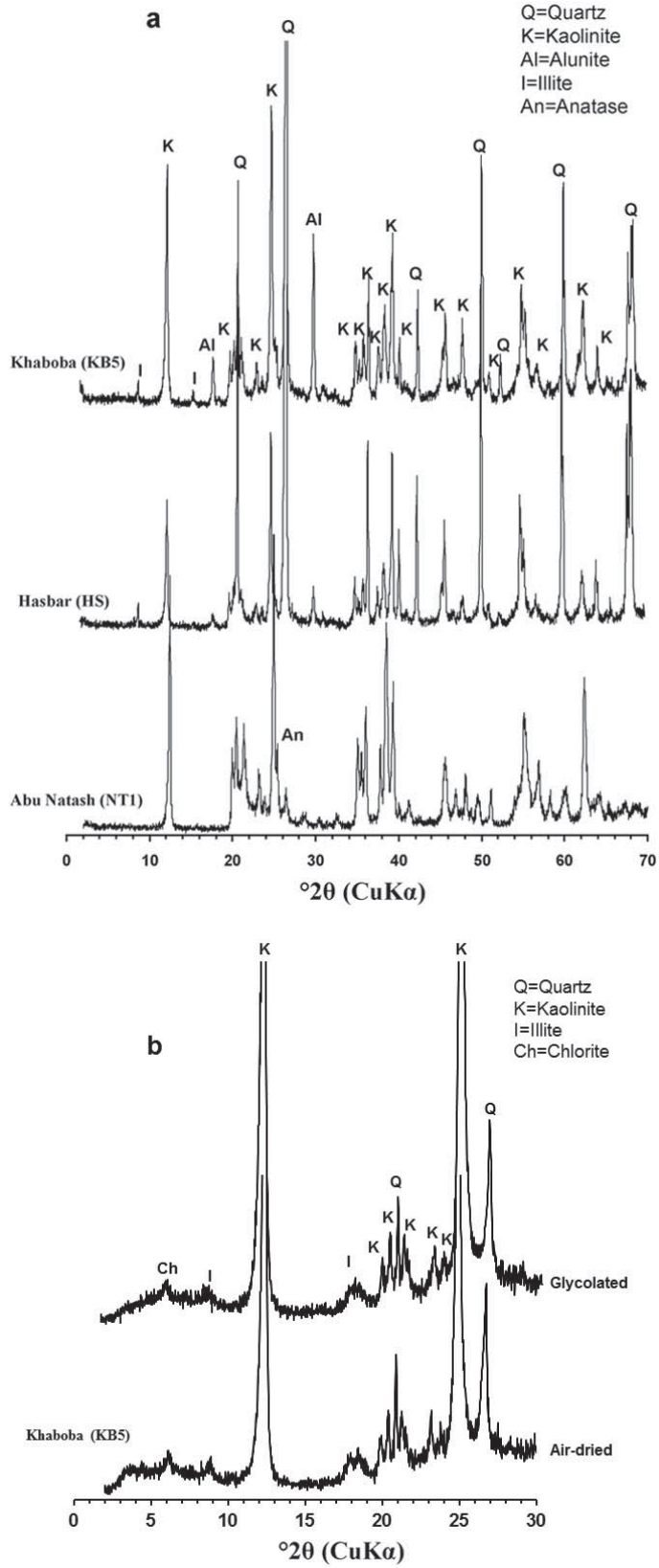

Figure 8. XRD patterns of representative bulk samples (Abu Natash, Hasbar, and Khaboba areas) (a) and clay fractions (Khaboba deposit) (b) from the Carboniferous kaolin deposits in Sinai.

Table 2. Mineralogical compositions (wt.%) and geochemistry of major oxides (wt.%), trace elements (ppm), and *REE* (ppm) of the clay fractions from the Carboniferous kaolin deposits, Sinai.

Sample	KB1	KB2	KB3	KB5	KB7	HS	NT1	NT2	NT3
Kaolinite	85	78	80	83	78	61	94	96	95
Quartz	9	15	9	10	13	31	2	T	nd
Anatase	2	2	2	2	2	2	5	3	4
Alunite	1	1	5	1	1	3	nd	nd	nd
Illite	2	2	2	2	2	3	nd	nd	nd
Chlorite	nd	1	1	1	2	nd	nd	nd	nd
Microcline	T	T	T	T	T	T	nd	nd	nd
Hinckley Index	0.85	0.68	0.61	0.80	0.60	0.82	0.70	0.72	0.73
SiO_2	50.20	53.87	44.56	48.69	51.28	67.54	43.00	43.24	42.92
TiO_2	1.61	1.70	1.55	1.49	1.60	1.58	4.32	3.15	3.50
Al_2O_3	33.33	30.50	34.34	34.30	32.65	17.92	37.50	37.68	37.86
Fe_2O_3*	0.62	1.08	0.89	1.07	0.86	0.64	0.76	0.72	1.07
MnO	bdl	bdl	bdl	bdl	bdl	bdl	bdl	bdl	bdl
MgO	0.30	0.39	0.35	0.44	0.36	0.27	0.30	0.18	0.19
CaO	0.08	0.07	0.05	0.08	0.11	0.18	0.08	0.04	0.06
Na_2O	0.15	0.16	0.31	0.18	0.14	0.18	0.06	0.05	0.19
K_2O	0.69	0.95	1.55	0.91	0.78	0.94	0.01	0.00	0.01
P_2O_5	0.07	0.08	0.08	0.07	0.07	0.17	0.23	0.09	0.10
LOI	12.76	10.70	15.48	12.23	11.65	10.32	13.70	13.85	13.43
Sum	99.80	99.51	99.18	99.45	99.51	99.75	99.96	99.00	99.33
Si/Al	1.51	1.77	1.30	1.42	1.57	3.77	1.15	1.15	1.13
Ba	181	239	246	219	213	245	69	42	49
Co	bdl	bdl	bdl	bdl	bdl	bdl	2	0.8	1.5
Cr	98	100	108	118	109	57	221	362	312
Cs	6		6	7.8	9.4	5.7	bdl	0.1	bdl
Hf	6		7	5.4	8.2	11.7	5.7	5. 1	4.2
Li	71		181	273	254	26	82	58	56
Nb	59	61	56	53	59	63	61	36	43
Ni	40	60	38	42	48	27	0	15	3
Pb	29		26	26	25	50	203	155	181
Rb	30		45	35	44	55	0.3	0.6	0.3
Sr	115	136	233	122	115	345	721	288	298
Ta	3		3	2	3	4	2	2	2
Th	15		18	14	19	30	6	3	4
U	4		6	4	6	10	4	2	2
V	201	167	202	169	161	120	429	331	382
Y	49	63	50	47	53	94	35	23	33
Zn	bdl	11	21	18	bdl	bdl	bdl	bdl	26
Zr	355	389	325	291	339	468	468	165	174
La	47.3		74.3	53	80.2	125	167	32.1	54.9
Ce	105		148	103	156	282	327	72.4	132
Pr	10.6		15.5	10.3	16.1	38.9	40.8	9.3	17.9
Nd	34.2		48.9	32.3	53.0	180	171	39.3	78.9
Sm	4.5		5.3	4.3	8.09	53.3	32.6	7.9	15.3
Eu	0.8		0.9	0.7	1.4	8.66	7.7	1.8	3.9
Gd	3.4		3.7	3.2	6.3	32.1	20.7	5.5	10.8
Tb	0.7		0.8	0.6	1.1	3.46	2.1	0.6	1.1
Dy	4.8		5.8	4.2	7.3	17.9	9.0	3.4	5.2
Ho	1.0		1.3	0.9	1.5	3.56	1.34	0.7	1.1
Er	2.9		3.70	2.8	4.5	10.1	3.34	2.2	3.4
Tm	0.5		0.6	0.4	0.6	1.4	0.44	0.3	0.5
Yb	2.9		3.6	2.6	4.3	9.3	2.81	2.2	3.8
Lu	0.4		0.5	0.4	0.64	1.34	0.45	0.35	0.60
Eu/Eu^*_{CN}	0.59		0.59	0.57	0.59	0.64	0.91	0.93	0.92
$(La/Yb)_{CN}$	10.9		13.9	13.7	12.6	10.6	40.1	9.9	9.8
Eu/Eu^*_{SN}	0.90		0.90	0.87	0.91	0.98	1.39	1.28	1.40
Gd/Gd^*_{SN}	0.65		0.51	0.61	0.75	2.13	2.05	1.41	1.62
$(La/Yb)_{SN}$	1.19		1.51	1.49	1.38	0.99	4.38	1.08	1.07

CN = Chondrite-normalized; SN = Shale (PAAS)-normalized
T = trace: bdl = below detection level

Table 3. Grain-size distribution (wt.%), mineralogical compositions (wt.%), geochemistry of major oxides (wt.%), and alteration indices and trace elements (ppm) of the bulk samples of the Cretaceous kaolin deposits, Sinai.

Sample	TEH2	TEH3	TEH5	TEH8	TEH9	TEH10	KHA2	KHA4	KHB2	KHB4	KHB7
Sand		0.5		0.7	2.5	0.9	1.3			1.7	0.4
Silt		11.6		15.7	16.9	1.7	7.1			3.3	7.0
Clay		87.9		83.6	80.7	97.4	91.6			95.0	92.7
Kaolinite	73	61	96	74	51	95	81	46	77	90	84
Quartz	24	35	1	23	46	2	15	51	20	7	12
Microcline	T	T	T	T	T	T	T	T	T	T	T
Anatase	2	3	2	2	2	2	2	2	2	2	3
Hematite	T	nd	nd	nd	T	nd	1	T	nd	T	nd
SiO_2	55.3	61.5	44.1	50.18	68.60	44.9	50.9	70.97	51.96	46.86	48.4
TiO_2	2.42	2.62	2.28	2.26	2.00	1.56	2.05	1.71	2.23	1.88	3.52
Al_2O_3	28.6	24.1	37.8	29.78	20.17	38.9	31.97	18.13	30.57	35.43	33.42
Fe_2O_3*	1.31	1.09	1.15	1.07	1.24	1.09	2.83	1.72	1.19	1.79	1.13
MnO	0.01	0.01	0.01	0.01	0.01	0.0	0.01	0.01	0.01	0.0	0.0
MgO	0.21	0.20	0.26	0.22	0.16	0.23	0.23	0.17	0.29	0.24	0.24
CaO	0.05	0.05	0.09	0.16	0.06	0.05	0.12	0.05	0.28	0.08	0.09
Na_2O	0.10	0.10	0.16	0.09	0.08	0.18	0.11	0.09	0.13	0.10	0.11
K_2O	0.10	0.16	0.02	0.08	0.02	0.03	0.04	0.06	0.04	0.07	0.04
P_2O_5	0.08	0.08	0.08	0.11	0.06	0.12	0.07	0.07	0.07	0.09	0.09
LOI	11.0	10.1	14.2	15.95	8.56	14.1	11.80	7.53	14.10	13.52	13.30
Sum	99.2	100	100	99.9	101	100	100.1	100.5	100.9	100.1	100.3
Ba	114	123	63	315	119	117	76	100	86	110	111
Co	bdl	bdl	5	4	4	2	6	1	1	1	bdl
Cr	127	143	138	144	86	127	171	110	127	128	125
Nb	103	101	126	107	84	105	78	56	86	93	127
Ni	85	81	121	88	103	77	87	83	90	105	97
Rb	3	4	bdl	bdl	bdl	bdl	bdl	3	bdl	bdl	bdl
Sr	105	89	67	190	66	158	93	73	101	177	178
V	143	150	184	192	155	193	223	135	145	159	128
Y	76	109	94	80	60	115	71	60	55	60	59
Zn	17	13	54	15	34	88	93	25	69	46	28
Zr	707	765	718	710	622	631	503	656	597	550	694
CIA	99.1	98.6	99.3	99.1	99.4	99.2	99.1	98.8	98.1	99.3	99.3
ICV	0.15	0.18	0.11	0.13	0.18	0.08	0.17	0.21	0.14	0.12	0.15

contains less Al_2O_3 (~15 wt.%) than the Khaboba and Abu Natash deposits (averages of 25 and 37.6 wt.%, respectively). As a result of the large anatase contents, the Abu Natash deposit had greater TiO_2 contents (average of 3.2 wt.%) than the Khaboba and Hasbar deposits (averages of 1.5 and 1.4 wt.%, respectively). The clay fractions in all deposits showed slight increases in terms of Al_2O_3 and TiO_2 contents and decreases in the SiO_2 and Fe_2O_3 contents compared to the bulk samples due to smaller amounts of quartz and hematite. The Si/Al ratios of the clay fractions of the Khaboba and Hasber deposits (1.5 and 3.7, respectively) were greater than that of the typical kaolinite (1.17) due to the presence of quartz in the clay fractions, which was confirmed by the XRD analyses of these deposits. On the other hand, the Si/Al ratio of the clay fractions of the Abu Natash deposits was 1.15, which is very close to that of the typical kaolinite due to the absence of quartz in the clay fractions of this deposit. Among the Cretaceous deposits, bulk samples from the Sakar and Esela areas showed the greatest Al_2O_3 value (averages of 35 and 33 wt.%, respectively) and the smallest SiO_2 contents (averages of 47 and 49 wt.%, respectively) due to the greater kaolinite and smaller quartz contents. The clay fractions of all deposits revealed a slight increase in the Al_2O_3 and decrease in the SiO_2 contents compared to the bulk samples. The TiO_2 contents showed no major changes between the bulk samples and clay fractions due to the predominance of submicron-sized anatase. With few exceptions, the Si/Al ratios of the clay fractions of all deposits were very close to the Si/Al ratios of the typical kaolinite (1.17). The exceptionally high Si/Al ratios in some samples were due to the presence of quartz in the clay fractions.

The clay fractions from the Carboniferous kaolin deposits had, on average, more SiO_2 (average of 49 wt.%) than the Cretaceous deposits (average of 44.6 wt.%) due to their greater quartz contents in the

Table 3 continued

Sample	SK1	SK2	SK3	SK4	ES1	ES5	ES6	ES8	ES10	MS1	MS3	MS6	MS9
Sand		0.4	0.5		0.5	0.2	0.5	0.7	3.1	6.3	2.04	1.1	1.4
Silt		5.4	7.2		4.1	3.7	10.3	1.9	6.80	5.4	18.3	13.9	6.7
Clay		94.3	92.3		95.5	96.1	89.2	97.4	90.1	88.4	79.7	85.1	91.9
Kaolinite	87	87	88	90	84	94	71	95	83	75	55	47	82
Quartz	10	10	9	5	12	5	25	3	14	20	41	49	14
Microcline	T	T	T	2	T	T	T	T	T	T	T	1	T
Anatase	2	2	2	2	3	2	3	1	4	3	3	2	3
Hematite	nd	nd	T	T	T	nd	T	T	nd	T	T	T	T
SiO_2	48.3	47.14	47.8	45.6	50.53	45.3	53.7	45.7	49.9	53.5	63.6	70.3	51.9
TiO_2	2.04	2.06	1.91	2.01	2.69	1.89	2.73	1.31	4.45	2.84	2.80	1.74	2.98
Al_2O_3	34.7	34.60	34.8	35.7	33.42	36.7	28.2	37.9	32.5	28.7	21.8	18.3	32.6
Fe_2O_3*	1.53	1.62	1.79	1.93	1.42	1.51	4.16	0.99	1.16	0.69	2.18	1.01	1.27
MnO	bdl	bdl	bdl	bdl	0.01	bdl	0.01	bdl	0.01	0.01	0.01	0.01	0.01
MgO	0.27	0.32	0.28	0.25	0.23	0.37	0.25	0.25	0.21	0.20	0.19	0.19	0.22
CaO	0.08	0.17	0.11	0.12	0.04	0.07	0.07	0.11	0.05	0.09	0.03	0.02	0.04
Na_2O	0.12	0.44	0.13	0.11	0.08	0.10	0.11	0.13	0.09	0.12	0.11	0.10	0.10
K_2O	0.05	0.03	0.07	0.03	0.11	0.09	0.16	0.05	0.03	0.03	0.07	0.26	0.06
P_2O_5	0.04	0.05	0.05	0.05	0.08	0.18	0.13	0.16	0.08	0.07	0.11	0.09	0.13
LOI	13.2	13.86	13.3	14.7	12.29	13.9	10.4	13.56	11.8	13.8	8.44	7.31	11.9
Sum	100	100	100	100	100.9	99.9	99.8	99.9	100	100	99.2	99.3	100
Ba	54	65	45	43	106	172	138	147	72	310	112	137	140
Co	1	bdl	2	2	3	8	15	11	4	bdl	2	bdl	bdl
Cr	150	107	135	145	169	133	177	187	181	142	168	80	213
Nb	108	106	101	108	86	50	95	62	164	119	92	49	98
Ni	90	0	92	114	119	455	96	115	170	129	113	75	95
Rb	bdl	bdl	bdl	bdl	3	2	5	bdl	bdl	bdl	bdl	11	bdl
Sr	54	52	66	63	103	17	146	219	62	79	147	182	196
V	144	155	116	143	193	201	219	496	216	198	230	104	216
Y	58	22	53	68	57	450	113	61	79	72	66	61	90
Zn	16	18	18	22	28	43	152	58	41	4	17	bdl	2
Zr	619	588	592	660	564	152	609	479	1049	778	801	567	657
CIA	99.1	97.3	98.9	99.1	99.3	99.3	98.8	99.3	99.4	99.2	98.8	97.6	99.3
ICV	0.12	0.13	0.12	0.12	0.14	0.11	0.27	0.07	0.18	0.14	0.25	0.18	0.14

THE = Teeh deposit
KHA and KHB = Kheel deposit bed A and bed B, respectively
SK = Sakar deposit
ES = Esela deposit
MS = Mosabaa deposit

clay fractions. On the other hand, Al_2O_3 was greater in the Cretaceous deposits (average of 36.7 wt.%) than in the Carboniferous deposits (averages of 33 wt.%) as a result of more kaolinite in the clay fractions of the Cretaceous deposits. No correlations were observed between Al_2O_3 and either Fe_2O_3 or TiO_2 in the bulk samples or clay fractions of all Carboniferous and Cretaceous deposits, suggesting the small possibility that Fe and Ti substituted for Al in the kaolinite structure in these deposits.

Trace elements. Trace-element distributions in both bulk samples and clay fractions of the Carboniferous and Cretaceous deposits (Tables 1–4) showed that elements such as Ba, Li, Cr, Sr, V, and Zr occurred in most of the deposits in relatively high concentrations (>100 ppm) and elements such as Nb, Ni, Y, and Pb occurred in intermediate concentrations (20–100 ppm), while elements such as Co, Cs, Rb, Hf, Ta, and U occurred in relatively small concentrations (<20 ppm) in both bulk deposits and clay fractions. With the exception of unusually high Li contents, these compositional ranges were within the expected ranges for shales in general (*e.g.* Turekian and Wedepohl, 1961; Gromet *et al.*, 1984; Taylor and McLennan, 1985) and kaolins (*e.g.* McLaughlin, 1959; Kogel and Lewis, 2001; Sousa *et al.*, 2007).

Among the Carboniferous deposits, the clay fractions from the Abu Natash deposit had lower concentrations of Ba, Co, Cs, Nb, Rb, Y, Zr, Hf, Ta, Th, and U and greater Cr, Sr, V, and Pb contents than the Khaboba and Hasbar deposits. The Hasbar deposit had larger Ba, Nb, Y, Zr, Hf, Ta, Th, and U and smaller Cr, Li, V, and Zn contents

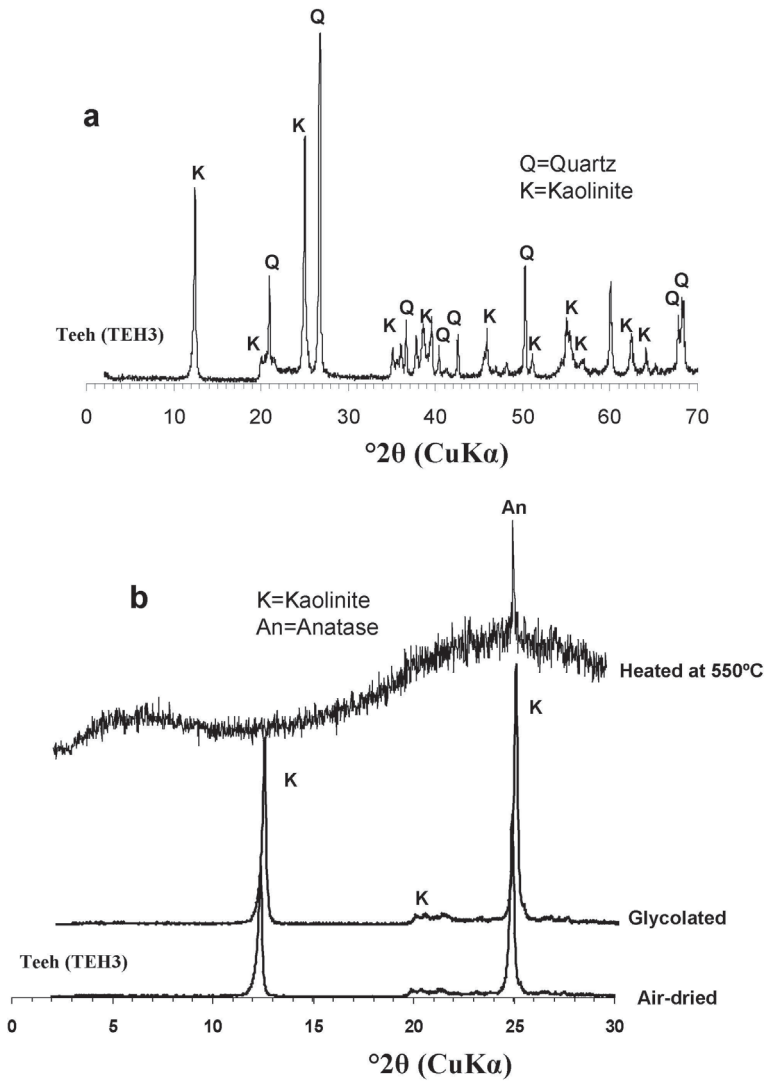

Figure 9. XRD patterns of a representative bulk sample (a) and clay fractions (b) from the Cretaceous kaolin deposits in Sinai (Teeh deposit).

than the Khaboba and Abu Natash deposits. The Khaboba deposit had greater Co, Cs, Li, and Rb and smaller Sr and Pb concentrations than the Hasbar and Abu Natash deposits.

The Cretaceous deposits are generally homogeneous and only slight variations in the distribution of trace elements in both the bulk deposits and clay fractions can be observed among the different deposits. For example, the Sakar deposit was characterized by smaller Ba, Sr, Pb, and Th contents than the other Cretaceous deposits. In samples from the Mosabaa deposit, the amounts of Nb and Sr were slightly greater and Zn was lower than in the other Cretaceous deposits.

None of the measured trace elements in either the bulk or clay fractions of any of the deposits correlated with SiO_2, Al_2O_3, or Fe_2O_3, indicating that none of these elements was related to quartz, kaolinite, or hematite, respectively. On the other hand, some of the trace elements, such as Cr, Nb, and Zr, showed positive correlations with TiO_2, indicating the association of these elements with TiO_2 in the anatase. Phosphate minerals (probably aluminum phosphate) appeared to hold some of the trace elements, such as Sr, Pb, and Th, as indicated by the positive correlations between P_2O_5 contents and these elements in the clay fractions of the studied deposits.

The results of the laser ablation analysis of 42 rutile grains separated from the sand fractions of the Cretaceous kaolin deposits indicated that the Cr contents ranged between 927 and 9140 ppm, while Nb contents were between 296 and 6555 ppm. With few exceptions, rutile grains were plotted in the field of metamafic source (Figure 10) in the Cr-Nd plot of Zack *et al.* (2004). Samples which plotted close to the dividing line

Table 4. Mineralogical compositions (wt.%) and geochemistry of major oxides (wt.%), trace elements (ppm), and *REE* (ppm) of the clay fractions from the Cretaceous kaolin deposits, Sinai.

Sample	TEH3	TEH8	TEH9	TEH10	KHA2	KHB4	KHB7	SK2	SK3
Kaolinite	90	87	88	95	90	91	90	94	94
Quartz	5	10	9	2	6	6	6	3	3
Microcline	1	T	T	T	T	T	T	T	T
Anatase	3	2	2	2	2	2	3	2	2
Hematite	T	T	T	T	1	T	nd	nd	T
Hinckley Index	0.77	0.64	0.74	0.66	0.51	0.65	0.57	0.52	0.61
SiO_2	45.78	46.90	45.20	44.30	45.18	45.70	44.50	44.46	45.06
TiO_2	2.58	2.10	2.14	1.74	1.89	1.78	2.85	1.61	1.70
Al_2O_3	36.22	33.89	35.16	37.93	35.80	36.03	36.25	37.65	36.73
Fe_2O_3*	1.39	1.08	2.32	1.02	2.77	1.69	1.19	1.59	1.72
MnO	0.01	0.01	0.01	bdl	bdl	bdl	bdl	bdl	bdl
MgO	0.25	0.22	0.21	0.28	0.26	0.26	0.23	0.25	0.24
CaO	0.06	0.16	0.10	0.14	0.16	0.11	0.12	0.11	0.11
Na_2O	0.06	0.05	0.05	0.06	0.06	0.06	0.06	0.06	0.06
K_2O	0.17	0.09	0.02	0.01	0.03	0.07	0.03	0.03	0.06
P_2O_5	0.13	0.12	0.09	0.12	0.07	0.10	0.08	0.04	0.04
LOI	12.97	14.88	14.43	13.62	13.15	13.49	14.22	13.63	13.65
Sum	99.61	99.47	99.71	99.22	99.37	99.28	99.53	99.42	99.39
Si/Al	1.26	1.38	1.29	1.17	1.26	1.27	1.23	1.18	1.23
Ba	149	229	171	111	68	109	92	32	49
Co	bdl	1.8	11	6	5	0.7	0.8	1.5	1.3
Cr	136	138	88	125	149	130	120	120	131
Cs	0.7	0.2	bdl	bdl	0.1	bdl	bdl	0.3	0.3
Hf	16.6	12.2	10.8	16.3	8.41	10.5	11.8	10.0	11.8
Li	76	62	59	117	77	78	123	143	116
Nb	118	100	99	122	78	88	109	93	96
Ni	73	87	73	93	88	75	82	82	95
Pb	29	29	29	31	22	24	34	10	26
Rb	5	3	0.6	0.4	0.7	2	0.7	0.6	0.8
Sr	168	187	105	158	101	179	166	51	66
Ta	7	5	5	7	3	4	6	5	5
Th	17	22	11	18	12	16	15	11	10
U	5	6	6	6	3	2	3	2	3
V	199	188	288	210	184	136	98	137	109
Y	150	67	64	139	73	62	53	48	56
Zn	5	9	71	112	96	48	22	30	28
Zr	665	590	520	742	463	530	584	477	532
La	82.8	77.3	55.6	66.6	46.2	50.9	45.4	21.3	9.7
Ce	166	129	97.5	138	84.6	102	83.0	46.4	20.9
Pr	18.4	14.2	10.5	17.5	9.51	11.8	9.8	5.03	1.9
Nd	72.3	51.6	35.8	78.1	36.3	45.3	37.6	20.3	6.5
Sm	13.8	10.1	7.2	19.2	7.4	9.5	7.4	4.3	1.6
Eu	2.9	1.9	1.6	4.1	1.6	1.9	1.5	0.8	0.4
Gd	14.5	7.7	6.7	17.4	7.5	7.5	5.7	3.9	2.3
Tb	2.9	1.3	1.2	2.9	1.4	1.1	0.9	0.7	0.4
Dy	19.0	8.0	7.5	18.5	9.3	7.1	6.1	4.6	3.3
Ho	3.9	1.5	1.5	3.6	1.8	1.4	1.3	1.0	0.7
Er	10.6	4.5	4.4	9.6	5.1	3.9	3.9	2.9	2.2
Tm	1.4	0.6	0.7	1.3	0.7	0.6	0.5	0.4	0.3
Yb	8.5	4.3	4.2	8.0	4.7	3.8	3.7	2.9	2.3
Lu	1.2	0.6	0.6	1.1	0.7	0.6	0.5	0.5	0.3
Eu/Eu^*_{CN}	0.63	0.67	0.71	0.69	0.66	0.71	0.70	0.60	0.63
$(La/Yb)_{CN}$	6.6	12.3	8.9	5.6	6.6	9.0	8.3	5.0	2. 9
Eu/Eu^*_{SN}	0.97	1.03	1.09	1.05	1.01	1.09	1.08	0.92	0.96
Gd/Gd^*_{SN}	1.25	0.95	0.97	1.72	1.13	1.20	1.01	1.09	1.10
$(La/Yb)_{SN}$	0.72	1.34	0.97	0.61	0.73	0.98	0.91	0.55	0.31

Table 4 continued

Sample	ES1	ES5	ES6	ES8	ES10	MS1	MS3	MS6	MS9
Kaolinite	95	93	88	96	95	94	93	93	95
Quartz	2	4	8	2	1	2	3	3	1
Microcline	T	T	T	T	T	T	T	T	T
Anatase	2	2	3	1	3	3	3	3	3
Hematite	nd	T	nd	T	nd	nd	nd	T	T
Hinckley Index	0.62	0.76	0.73	0.86	0.53	0.82	0.75	0.71	0.84
SiO_2	44.25	44.42	43.28	45.06	43.83	43.61	43.69	44.65	43.90
TiO_2	1.95	1.94	2.43	1.39	3.06	3.05	2.74	3.07	2.84
Al_2O_3	37.54	37.38	35.14	38.00	37.82	37.24	36.86	36.75	37.32
Fe_2O_3*	1.39	1.44	3.68	1.14	1.21	0.80	2.50	1.18	1.45
MnO	0.01	bdl	0.01	bdl	0.01	bdl	bdl	0.01	bdl
MgO	0.23	0.28	0.26	0.25	0.22	0.21	0.20	0.21	0.21
CaO	0.03	0.07	0.07	0.09	0.05	0.03	0.09	0.05	0.05
Na_2O	0.05	0.08	0.06	0.08	0.05	0.07	0.07	0.07	0.07
K_2O	0.09	0.09	0.12	0.03	0.02	0.02	0.06	0.05	0.04
P_2O_5	0.08	0.19	0.16	0.14	0.07	0.08	0.15	0.17	0.17
LOI	13.78	13.84	13.35	13.78	13.57	14.28	13.28	13.51	13.43
Sum	99.40	99.72	98.56	100.0	99.9	99.40	99.62	99.71	99.49
Si/Al	1.18	1.19	1.23	1.19	1.16	1.17	1.19	1.21	1.18
Ba	101	215	143	142	61	143	146	160	175
Co	4.4	11.9	13.3	11.1	6.2	bdl	1.5	bdl	bdl
Cr	163	160	183	192	136	143	180	186	211
Cs	0.6			0.2	0.1	0.1	0.1	0.1	
Hf	10.1			9.84	13.9	11.5	13.2	12.5	
Li	103.9			121.3	147.5	105.7	43.58	51.72	
Nb	74.0	80.6	104.8	70.3	134.9	123.4	107.3	103.1	107
Ni	77	68	94	134	153	84	77	73	43
Pb	28.3			34.1	24.4	26.0	33.9	36.8	
Rb	2.0			0.7	0.5	0.5	2.0	1.3	
Sr	115	228	226	183	72	82	271	346	292
Ta	4.1			3.1	6.6	6.1	5.0	5.4	
Th	6.7			24.3	11.5	13.5	17.4	18.8	
U	1.7			3.1	3.1	6.8	4.7	3.7	
V	143	171	209	441	166	211	266	182	216
Y	49	83	147	59	67	49	70	75	100
Zn	45	109	114	73	54	0	15	bdl	bdl
Zr	444	499	620	492	751	609	634	585	636
La	50.6			68.4	32.2	40.5	61.8	108	
Ce	90.6			153	56.5	71.0	124	223	
Pr	11.2			17.9	5.8	6.7	13.3	25.6	
Nd	44.3			69.9	19.2	22.3	47.5	101	
Sm	9.2			12.0	3.9	4.3	8.5	21.3	
Eu	2.1			2.2	0.9	1.0	1.7	4.5	
Gd	8.2			7.9	4.3	4.1	6.6	16.7	
Tb	1.3			1.3	0.8	0.8	1.1	2.1	
Dy	7.8			7.6	6.1	5.3	7.1	11.7	
Ho	1.5			1.5	1.3	1.1	1.5	2.3	
Er	4.0			3.9	3.6	3.3	4.4	6.4	
Tm	0.6			0.5	0.5	0.5	0.7	0.9	
Yb	3.6			3.5	3.7	3.3	4.5	6.0	
Lu	0.5			0.5	0.5	0.5	0.7	0.9	
Eu/Eu^*_{CN}	0.73			0.70	0.70	0.71	0.70	0.73	
$(La/Yb)_{CN}$	9.6			13.3	5.9	8.4	9.2	12.2	
Eu/Eu^*_{SN}	1.12			1.07	1.06	1.08	1.07	1.11	
Gd/Gd^*_{SN}	1.39			1.17	0.91	0.81	0.88	1.48	
$(La/Yb)_{SN}$	1.05			1.45	0.65	0.92	1.01	1.33	

bdl = below detection level; nd = not determined
T = trace

between the metamafic and metapelitic sources may be due to mixed sources.

Rare earth elements. Fine-grained sedimentary rocks often show *REE* distribution patterns that are very similar to that of average upper continental crust (*e.g.* McLennan, 1989). In a chondrite-normalized diagram, post-Archean shales are generally characterized by a light *REE* (*LREE*) enrichment over heavy *REE* (*HREE*) and a negative Eu anomaly (Gromet *et al.*, 1984; Haskin and Haskin, 1966; Nance and Taylor, 1976). Deviations from this pattern are expected when either specific source rocks and/or alteration in the form of more intense weathering or a hydrothermal or diagenetic overprint are involved (*e.g.* McLennan, 1989) and best visualized in shale-normalized (SN) diagrams.

The total *REE* content in each the clay fractions of the kaolin deposits studied (Tables 2, 4) was very variable (53 to 786 ppm), but was mostly greater than average shales (130–200 ppm; Gromet *et al.*, 1984; Haskin and Haskin, 1966; Nance and Taylor, 1974), indicating *REE*-enriched source lithologies and/or an enrichment process during intense weathering (kaolinization) (Cullers *et al.*, 1975; McLennan *et al.*, 1990; Condie, 1991). The kaolin deposits displayed no major Ce anomalies (Ce/Ce^*_{SN} = 0.94 to 1.17).

Chondrite-normalized *REE* patterns of the clay fractions from the Carboniferous deposits in the Khaboba and Hasbar areas (Figure 11a) exhibited *LREE* enrichment relative to *HREE*, as shown by the $(La/Yb)_{CN}$ ratio, which varied from 10.6 to 13.9, and the negative Eu anomaly with Eu/Eu^*_{CN} = 0.59–0.64. Although the chondrite-normalized *REE* patterns of the Abu Natash deposits showed relative enrichment of *LREE* compared to the *HREE* ($(La/Yb)_{CN}$ = 9–40), no negative Eu anomaly was observed (Eu/Eu^*_{CN} = 0.93). The Carboniferous kaolin deposits revealed distinct shale (PAAS)-normalized *REE* patterns that are characteristic of each deposit (Figure 11b). The clay fractions from the Khaboba deposit had a slight *LREE* over *HREE* fractionation ($(La/Yb)_{SN}$ = 1.19–1.51) with total concentrations only slightly above PAAS, but had a characteristic middle *REE* (*MREE*) depletion (Gd/Gd^*_{SN} = 0.51–0.75) and no Eu anomaly. In contrast, the kaolin deposits from Abu Natash showed a *MREE* enrichment (Gd/Gd^*_{SN} = 1.41–2.05) and a significant positive Eu anomaly (Eu/Eu^*_{SN} = 1.28–1.40). The Abu Natash kaolin deposits had very variable total *REE* concentrations (178–786 ppm). Most samples showed no *LREE* over *HREE* fractionation, only a single sample with the greatest *REE* content (NT1) was enriched in *LREE* ($(La/Yb)_{SN}$ = 4.19). A single sample from the Hasbar deposit had the greatest *MREE* enrichment (Gd/Gd^*_{SN} = 2.13) of all the investigated kaolin deposits, no *LREE* enrichment, or Eu anomaly, but large total *REE* contents.

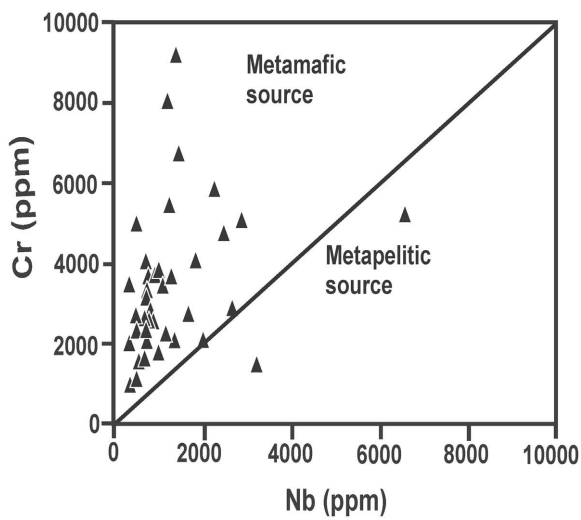

Figure 10. Cr-Nd plot of the rutile grains from the sand fractions of the Cretaceous deposits. With few exceptions, rutile was plotted in the field of mafic metamorphic field (reprinted from Zack, T., von Eynatten, H., and Kronz, A. (2004) Rutile geochemistry and its potential use in quantitative provenance studies, **171**, 1–4. © 2004, with permission from Elsevier).

Rare-earth element distributions in the clay fractions of the Cretaceous kaolin deposits (Table 4) showed that the Teeh deposits had the greatest *REE* contents (average ΣREE = 338 ppm), while the Sakar deposit had the smallest *REE* contents (average ΣREE = 84 ppm). Chondrite-normalized *REE* patterns for all Cretaceous kaolin deposits (Figure 11c) exhibited L*REE* enrichment relative to *HREE*, as shown by the $(La/Yb)_{CN}$ ratio, which varied from 2.9 to 13.3, and the negative Eu anomaly with Eu/Eu^*_{CN} = 0.60 to 0.73. The Sakar deposit had the smallest $(La/Yb)_{CN}$ values (2.9–5), and the strongest Eu negative anomaly with Eu/Eu^*_{CN} = 0.60–0.63. On the other hand, the deposit of the Mosabaa area had the greatest $(La/Yb)_{CN}$ values (8.3–12.2) and the weakest Eu negative anomaly (Eu/Eu^*_{CN} = 0.70 to 0.73). Most of the Cretaceous deposits showed flat shale (PAAS)-normalized patterns with slight L*REE* depletions or enrichments ($(La/Yb)_{SN}$ = 0.6 to 1.4) and a moderate *MREE* enrichment (Gd/Gd^*_{SN} = 0.88–1.39) in some samples (Figure 11d). A clear exception was the Sakar deposit with very low total *REE* contents, low $(La/Yb)_{SN}$ values (0.3–0.5), weak negative Eu (Eu/Eu^*_{SN} = 0.92–0.96), and slight positive Ce (Ce/Ce^*_{SN} = 1.09–1.17) anomalies.

Light rare-earth elements (La, Ce, Pr, Nd, and Sm) represented the major fraction of the rare-earth elements (80–90% of the total *REE* concentrations) in all deposits. The total *REE* values showed a positive correlation with P_2O_5 contents in the clay fractions of all the kaolin deposits (Figure 12), indicating the occurrence of most of these elements in the phosphate minerals. Monazite was also identified in the Khaboba deposit by SEM and could also be a host of the *REE*; the chondrite-normalized *REE* pattern of this deposit, in particular, was similar to that of monazite (*e.g.* Nagy *et al.*, 2002).

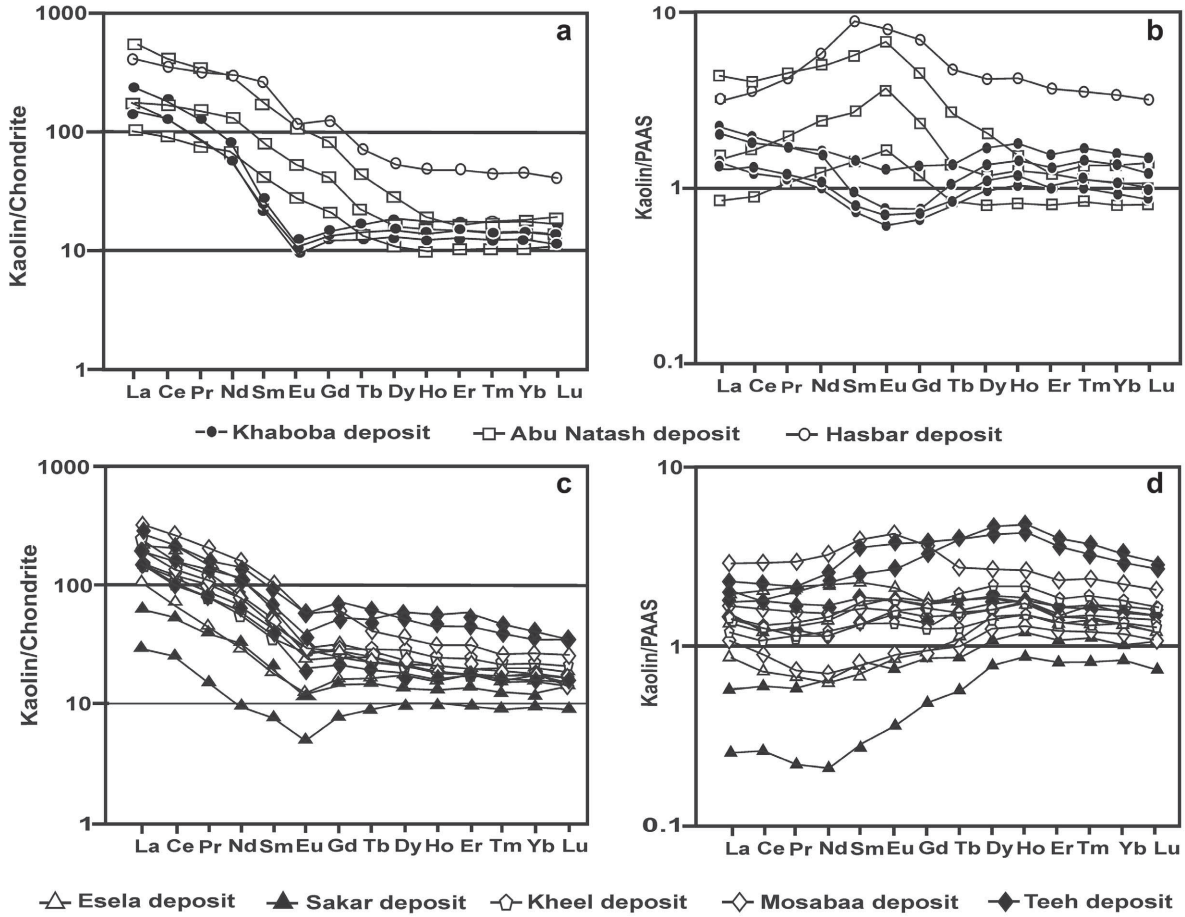

Figure 11. (a) Chondrite-normalized *REE* patterns (using chondrite *REE* concentrations provided by Boynton (1984)) and (b) shale (PAAS)-normalized *REE* patterns (using PAAS *REE* concentrations provided by Nance and Taylor (1976)) of the clay fractions from the Carboniferous kaolin deposits. (c, d) Chondrite- and shale (PAAS)-normalized *REE* patterns of the clay fractions from the Cretaceous deposits.

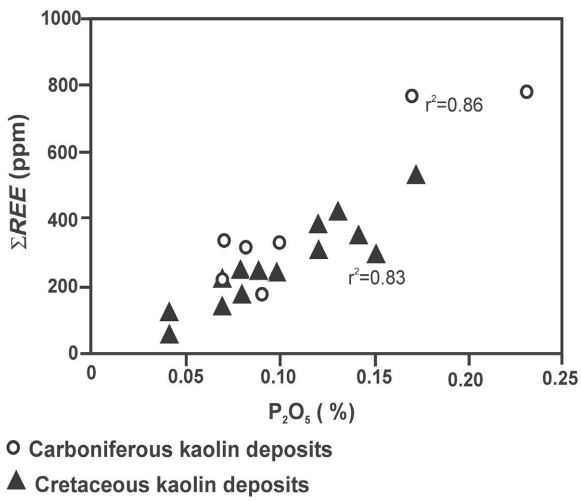

Figure 12. P_2O_5-Σ*REE* binary plot of the clay fractions in the Carboniferous and Cretaceous kaolin deposits. Both deposits show strong positive correlations between the P_2O_5 contents and Σ*REE*.

DISCUSSION

The mineralogical and geochemical variations between kaolin deposits of different ages in the same region and also among deposits of the same age were remarkable and suggested that the source-area composition played a role in these variations. Variable degrees of weathering, both in the source regions and after deposition of the clays, were considered to be minor factors, as the various chemical indices of alteration or weathering were very similar and high for most deposits. Ferruginous laterites were reported from the Triassic Wadi Budra formation in SW Sinai (Goldbery and Beyth, 1984) and lateritic gibbsite-bearing shales in the Carboniferous Um Bogma formation (El Hazek *et al.*, 2008). However, note that clear evidence for a laterite-derived facies, such as strong *LREE* depletions with concomitant large positive Ce anomalies, etched quartz grains, or pisolitic textures characteristic of Lower Cretaceous flint kaolin deposits of the Kalabsha deposit, southern Egypt (Baioumy and Gilg, 2011), was absent

from the deposits investigated. Note also that no indications of hydrothermal overprints, deep burial, or strong diagenesis were observed for either the Carboniferous or Cretaceous kaolin deposits. Thus, distinct lithologies in the source region were considered the key factors for the chemical and mineralogical differences observed in the Sinai kaolin deposits.

The kaolin deposits investigated are located at the northwestern edge of the Panafrican ANS, mostly at the periphery of the crystalline basement, but also partly within small grabens within the shield. Weathering crusts on the ANS, now eroded, were the main sources of the sedimentary protoliths of the kaolin deposits. Some minor contributions from weathered Paleozoic or Mesozoic sediments should not be excluded, though these were relatively small in volume and in most cases were also derived from the shield (*e.g.* Khalifa *et al.*, 2006; Kolodner *et al.*, 2009; Akarish and El-Gohary, 2008). The ANS in the Sinai at its present erosional level consists mainly of Neoproterozoic calc-alkaline to alkaline granitic rocks and juvenile mafic oceanic and mafic to felsic oceanic arc volcanics with minor sediments that are metamorphosed to greenschist–amphibolite-facies conditions (*e.g.* Beeri-Shlevin, 2009).

The mineralogical and geochemical heterogeneity was most prominent among the various Carboniferous kaolin deposits. The kaolin deposits from the Khaboba area were characterized by the presence of illite and chlorite in the clay fraction and the lack of rutile in the heavy mineral spectrum. The absence of rutile clearly indicated that medium- to high-grade mafic or sedimentary metamorphic rocks were lacking in the source area (Force, 1980, 1991). The scarce contribution of weathered mafic rocks was corroborated by the moderate Cr, V, and Ti concentrations in the kaolin. The presence of chlorite and illite, large Li, Rb, and Cs values, and shale-like La/Yb ratios rather suggested that weathering crusts on low-grade metasediments prevailed in the source region. At Wadi Khaboba, a few km south of the kaolin deposit, the contact between the Paleozoic sedimentary cover and basement is exposed. Chlorite- and biotite-rich micaschists predominate and still show a residual kaolinitic weathering cap, which is a few meters thick, at the contact with the overlying Paleozoic sediments. The *REE* content of the Khaboba kaolin deposits showed a characteristic, flat, shale-normalized pattern with a pronounced *MREE* depletion. Similar patterns have been encountered in the sedimentary kaolin deposits of the Capim area in northern Brazil (*e.g.* Sousa *et al.*, 2006, 2007), and the Eocene hard kaolin deposits of Georgia, USA (Kogel and Lewis, 2001), as well as weathered Silurian shale at the Susquehanna/Shale Hills Critical Zone Observatory, Pennsylvania, and many other locations world-wide (Ma *et al.*, 2011, and references therein). The depletion of *MREE* is generally related to the dissolution of phosphate minerals such as rhabdophane or Fe-Mn-hydroxides (Ma *et al.*, 2011). Whether this *MREE* depletion occurred during weathering of metasediments in the source region or during subsequent kaolinization after deposition of the clays is unclear. The occurrence of alunite in the Khaboba deposits, which might have formed by the oxidation of sulfides in the clays, may support the assertion that *MREE* depletion in these deposits occurred during subsequent kaolinization, after deposition of the clays.

The Abu Natash kaolin deposit is the only deposit in the Sinai with very small quartz contents. The deposit contains unusually large amounts of compatible elements such as Ti, Cr, V, and Sr, and generally small amounts of incompatible elements, especially Ba, Rb, Cs, Zr, and Th. These characteristics favor a significant mafic component in their source region. The absence of chondrite-normalized Eu anomalies, large La/Yb_{SN} values, and large Nb and Ta contents indicate that mafic alkaline rather than calc-alkaline arc magmas were involved (*e.g.* McLennan *et al.*, 1990; Prudêncio *et al.*, 1995; Plank and Langmuir, 1998). The unusually high Pb contents (155–403 ppm) were not compatible with mafic protoliths and required additional, possibly hydrothermal Pb mineralization in the source area. Note that the hydrothermal manganese deposits in the Carboniferous Um Bogma Formation showed significant Pb enrichment (*e.g.* Saad *et al.*, 1994; El-Agami *et al.*, 2000).

The single sample from the Hasbar kaolin deposit investigated here was distinct from both the Khaboba and Hasbar deposits in that it has a very large quartz content in the clay fraction, large mica-related element concentrations (K, Rb, Cs), and very large Th, Y, *REE*, and P values. These characteristics might indicate monazite- or xenotime-rich metasediments.

Unlike the Carboniferous kaolin deposits, the Cretaceous kaolin deposits are far less heterogeneous with respect to their chemical and mineralogical composition. Clay minerals other than kaolinite are lacking and the quartz contents of the clay fractions are much smaller than in the metasediment-sourced Carboniferous Khaboba and Hasbar kaolin deposits. Thus, low-grade metasediments were less abundant in the source area. The low silt + sand contents of the Cretaceous kaolin deposits also indicate more efficient particle-size sorting and probably greater transport distances than for the Carboniferous kaolin deposits. Both processes contributed to the observed homogenization. The very high CIA values (>98) demonstrated the maturity of the Cretaceous sedimentary kaolin deposits. The presence of rutile in the heavy mineral spectra is remarkable and implies a shift from low- to medium- or high-grade metamorphic source rocks. These mineralogical changes indicated either significant exhumation and erosional unroofing of the Arabian-Nubian Shield between Carboniferous and Cretaceous times, and/or a shift from rather local to larger, more regional sources

that include more medium/high-grade metamorphic rocks. The geochemical data indicated that diverse lithotypes were present in the source region of the clays.

Large Cr and small Nb contents of the rutile are indicative of a mafic rather than a metasedimentary source for this mineral. The presence of mafic source rocks was corroborated by high Ti, Cr, and V concentrations in the clay fractions. Nevertheless, the concentrations of the compatible elements were not as great as in the Carboniferous mafic-dominated Abu Natash kaolin deposits. The participation of granitic source materials was indicated by high Zr, *REE*, and Li, low Sr contents, and chondrite-normalized negative Eu anomalies of the Cretaceous sedimentary kaolin deposits. The unusually large Nb (70−135 ppm) and Ta contents and, in part, the small $(La/Yb)_{SN}$ ratios of the kaolin deposits might indicate Nb-Ta-mineralized, highly fractionated granitic, rhyolitic, or pegmatitic rocks in the source area. Bastnaesite inclusions were detected in a zircon crystal from the Cretaceous Teeh kaolin. Note that (per-)alkaline granitic rocks (*e.g.* Beeri-Shlevin, 2009; Eyal *et al.*, 2010) and even carbonatitic rocks (Shimron, 1975) exist on the Sinai peninsula.

The geochemical and mineralogical characteristics of the Lower Cretaceous kaolin deposits from Sinai are similar to the Upper Cretaceous plastic kaolin deposits of the Kalabsha district in southern Egypt, which were also derived from kaolinitic weathering crusts on the ANS (Baioumy and Gilg, 2011). The Kalabsha kaolin deposits have even greater Zr and Nb contents in the clay fraction than the Cretaceous Sinai kaolin deposits. These data suggest that the geochemical characteristics of the sedimentary kaolin deposits at the border of ANS are related to the specific composition of this Late Proterozoic juvenile crust with accreted oceanic arc terranes, with minor, low-grade metasediments and a few medium- to high-grade metamorphic core complexes, post-orogenic granitoids and volcanics, and some anorogenic alkaline igneous rocks.

The schematic diagrams of Figure 13 illustrate the possible sources and depositional settings of both the Carboniferous and Cretaceous kaolin deposits. During the Carboniferous, weathering crusts on low-grade metamorphic, granitic, and mafic alkaline rocks were eroded and deposited in local basins close to the source area. This resulted in mineralogically and geochemically heterogeneous and less mature kaolin deposits.

The source area for the Cretaceous kaolin deposits is considered much larger than that of the Carboniferous kaolin deposits. Medium- to high-grade metamorphic, mafic, granitic, and alkaline rocks of the ANS were exposed to weathering during the Jurassic and Lower Cretaceous. The saprolites were eroded and the suspended clays deposited in basins far away from the source area to form relatively homogeneous and textural and compositional mature kaolin deposits. Superimposed supergene diagenetic alteration, including kaolinization and deferration, probably contributed to economic sedimentary kaolin formation during both periods.

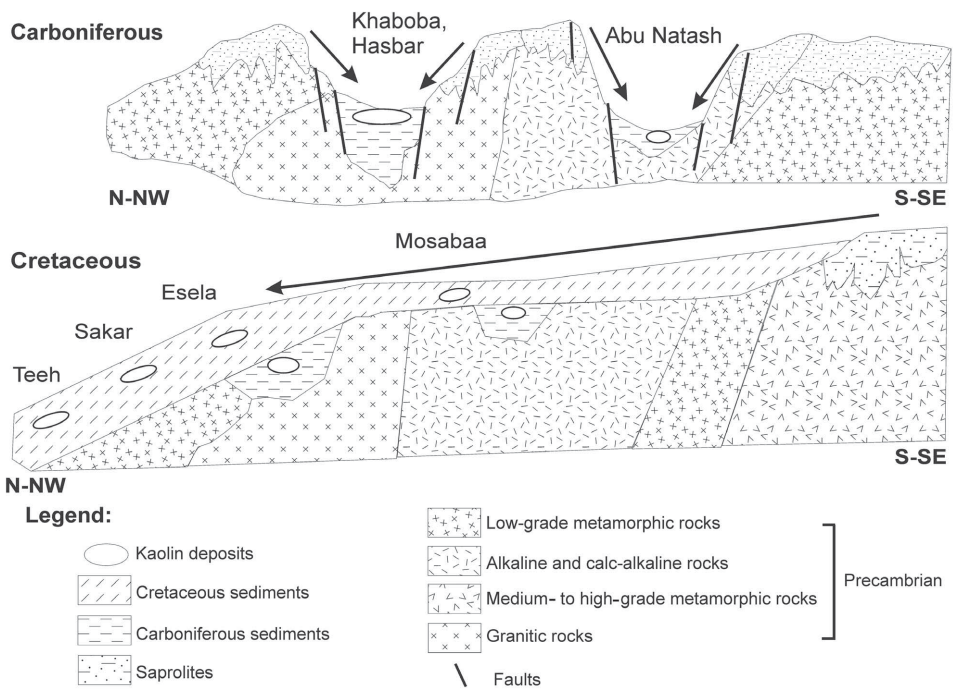

Figure 13. Schematic diagram showing the possible sources and formational mechanisms of the Carboniferous (a) and Cretaceous (b) kaolin deposits in Sinai. Arrows indicate the transportation direction of weathering products.

CONCLUSIONS

The present study demonstrated that combined mineralogical and geochemical studies on bulk samples and clay fractions of kaolin deposits, as well as on heavy-mineral fractions, yield import information regarding possible source lithologies for sedimentary kaolin deposits of the Sinai. The chemical heterogeneity of sedimentary kaolin deposits in such a small area at the northern border of the Arabian-Nubian Shield was unexpected. The predominance of low-grade metapelitic and mafic rocks in the source area was identified in two Carboniferous kaolin deposits, Khaboba and Hasbar, respectively, while rather well mixed source lithotypes of the Arabian Nubian Shield and probably longer transport paths were characteristic of the Lower Cretaceous kaolin deposits. The mineralogical and chemical data also gave some insight into the alteration history, such as the degree of weathering. At present, the relative proportions and intensities of kaolinization in the source region *vs. in situ* kaolin formation of the sedimentary clays cannot be assessed easily.

ACKNOWLEDGMENTS

The authors are grateful to the Alexander von Humboldt Foundation, Germany, which funded this work through the postdoctoral fellowship awarded to Hassan Baioumy. The staff of the geology group at Technische Universität München (TUM) are thanked for their technical support. The authors are also grateful to Dr Peter Dulski of Helmholtz-Zentrum GFZ in Potsdam for ICP-MS analyses, and to Dr Helene Brätz, Erlangen University, for LA-ICP-MS analyses on mineral separates. The authors also thank the Sinai Manganese Company of Egypt for their guidance and support during the field work. Prof. K. Germann is acknowledged for helpful discussions during preparation for the field work and throughout the study. Finally, thanks are also extended to the staff at the Center for Material Analysis (ZWL) in Lauf, Germany, for help with the FE-SEM work.

REFERENCES

Abdallah, A.M., Adindani, A., and Fahmy, N. (1963) *Stratigraphy of Upper Paleozoic Rocks, Western Side of the Gulf of Suez, Egypt*. Egyptian Geological Survey, 18 pp.

Aboul-Ela, N.M., Abdel-Gawad, G.I., and Saber, S.C. (1990) Contribution to the stratigraphy of Gebel El-Minshera area, northern Sinai, Egypt. Abstracts, 28th Annual Meeting, The Geological Society of Egypt, Cairo, 18 pp.

Abu-Zied, R.H. (2008) Lithostratigraphy and biostratigraphy of some Lower Cretaceous outcrops from Northern Sinai, Egypt. *Cretaceous Research*, **29**, 603–624.

Akarish, A.I.M. and El-Gohary, A.M. (2008) Petrography and geochemistry of lower Paleozoic sandstones, East Sinai, Egypt: Implications for provenance and tectonic setting. *Journal of African Earth Sciences*, **52**, 43–54.

Beeri-Shlevin, Y., Katzir, Y., and Valley, J.W. (2009) Crustal evolution and recycling in a juvenile continent: Oxygen isotope ratio of zircon in the northern Arabian Nubian Shield. *Lithos*, **107**, 169–184.

Baioumy, H. and Gilg, H.A. (2011) Pisolitic flint kaolin from Kalabsha, Egypt: A laterite-derived facies. *Sedimentary Geology*, **236**, 141–152.

Boulis, S.N. and Attia, A.K. (2001) Mineralogy and origin of Carboniferous and Cretaceous kaolin deposits from a number of localities in Egypt. Pp. 221–229 in: *Mineral Deposits at the Beginning of the 21st Century* (A. Piestrzyrisk, editor). Swets and Zeitinger Publications, Lisse, The Netherlands.

Boynton, W.V. (1984) Geochemistry of the *REE*: Meteorite studies. Pp. 63–114 in: *Rare Earth Element Geochemistry* (P. Henderson, editor). Elsevier, Amsterdam.

Condie, K.C. (1991) Another look at rare earth elements in shales. *Geochimica et Cosmochimica Acta*, **39**, 1691–1703.

Costa, M.L. and Moraes, E.L. (1998) Mineralogy, geochemistry and genesis of kaolin deposits from the Amazon region. *Mineralium Deposita*, **33**, 283–297.

Cullers, R.L., Chaudhuri, S., Arnold, B., Lee, M., and Wolf, C.W. (1975) Rare earth distributions in clay minerals and in the clay-sized fraction of the lower Permian Havensville and Eskridge shales of Kansas and Oklahoma. *Geochimica et Cosmochimica Acta*, **39**, 691–1703.

Dombrowski, T. and Murray, H.H. (1984) Thorium – a key element in differentiating Cretaceous and Tertiary kaolin deposits in Georgia and South Carolina. *Proceedings of 27th International Geological Congress*, **15**, 305–317.

El-Agami, N.L., Ibrahim, E.H., and Oda, H.H. (2000) Sedimentary origin of the Mn-Fe ore of Um Bogma, southwest Sinai: Geochemical and paleomagnetic evidence. *Economic Geology*, **95**, 607–620.

El Hazek, M.N., Ahmed, F.Y., El Kasaby, M.A., and Attia, R.M. (2008) Sulfuric acid leaching of polymetallic Abu Zeneima gibbsite-shale. *Hydrometallurgy*, **90**, 34–39.

El-Shishtawy, A.M., Salem, I.A., Al-Dosuky, B.T., El-Assy, I.E., and Aly, G.A. (2006) Carboniferous kaolin deposits: Its petrology, radioactivity and genesis, Sinai, Egypt. *International Conference on Geochemistry, Alexandria, Egypt*, **II**, 107–132.

El-Shishtawy, A.M., Al-Dosuky, B.T., Salem, I.A., El-Assy, I.E., and Aly, G.A. (2008) Mineralogical and geochemical characteristics of Cretaceous kaolin deposits from west central Sinai, Egypt. *9th International Conference on the Geology of the Arab World (GAW-9)*, pp. 130–148.

Elzea Kogel, J., Pickering, S.M., Shelobolina, E.S., Chowns, T.M., Yuan, J., and Avant, D.M. (2002) The Georgia Kaolin deposits: Geology and Utilization. *Society for Mining, Metallurgy, and Exploration, USA*, 96 pp.

Eyal, M., Litvinovsky, B., Jahn, B.M., Zanvilevich, A., and Katzir, Y. (2010) Origin and evolution of post-collisional magmatism: Coeval Neoproterozoic calc-alkaline and alkaline suites of the Sinai Peninsula. *Chemical Geology*, **269**, 153–179.

Force, E.R. (1980) The provenance of rutile. *Journal of Sedimentary Petrology*, **50**, 485– 488.

Force, E.R. (1991) Geology of titanium-mineral deposits. *Geological Society of America Special Paper*, **259**, 112 pp.

Galán, E., Aparicio, P., Gonzales, I., and Laiglesia, A. (1994) Influence of associated components of kaolin on the degree of disorder of kaolinite as determined by XRD. *Geologica Carpathica Clays*, **45**, 59–75.

Ghorab, M.A. (1961) Abnormal stratigraphic features in Ras Gharib Oilfield, Egypt. *Proceedings of the Third Arab Petroleum Congress, Alexandria, Egypt*, pp. 1–10.

Goldbery, R. and Beyth, M. (1984) Laterization and ground water alteration phenomena in the Triassic Budra Formation, south-western Sina. *Sedimentology*, **31**, 575–594.

Gromet, L.P., Dymek, R.F., Haskin, L.A., and Korotev, R.L. (1984) The North American Shale composite: its compilation, major and trace element characteristics. *Geochimica et Cosmochimica Acta*, **48**, 2469–2482.

Haskin, M.A. and Haskin, L.A. (1966) Rare Earths in European shales: a redetermination. *Science*, **154**, 507–509.

Hinckley, D. (1963) Variability in crystallinity values among the kaolin deposits of the Coastal Plain of Georgia and South Carolina. *Proceedings of the 11th International Conference of Clays and Clay Minerals*, pp. 229–235.

Hurst, V.J. and Pickering, S.M. (1997) Origin and classification of Coastal Plain kaolin deposits, southeastern USA, and the role of groundwater and microbial action. *Clays and Clay Minerals*, **45**, 274–285.

Khalifa, M.A., Soliman, H.E., and Wanas, H.A. (2006) The Cambrian Araba Formation in northeastern Egypt: Facies and depositional environments. *Journal of Asian Earth Sciences*, **27**, 873–884.

Kleeberg, R. and Bergmann, J. (1998) Quantitative Röntgenphasenanalyse mit den Rietveld-Programmen BGMN und AUTOQUANT in der täglichen Laborpraxis. Pp. 237–250 in: *Tone in der Geotechnik und Baupraxis* (K.H. Henning and J. Kasbohm, editor). Beiträge zur Jahrestagung Greifswald, Berichte der DTTG, Greifswald, Germany.

Knill, J.L. (1978) *Industrial Geology*. Oxford University Press, London, 344 pp.

Kogel, J.E. and Lewis, S.A. (2001) Baseline studies of the Clay Minerals Society source clays: chemical analysis by inductively coupled plasma mass spectroscopy (ICP-MS). *Clays and Clay Minerals*, **49**, 387–392.

Kolodner, K., Avigad, D., McWilliams, M., Wooden J.L., Weissbrod, T., and Feinstein, S. (2009) Provenance of north Gondwana Cambrian–Ordovician sandstone: U–Pb SHRIMP dating of detrital zircons from Israel and Jordan. *Geological Magazine*, **143**, 367–391.

Kora, M., El-Shahat, A., and Abu Shabana, M. (1994) Lithostratigraphy of the Mn-bearing Um Bogma Formation, west-central Sinai, Egypt. *Journal of African Earth Science*, **18**, 151–162.

Ma, L., Jin, L. and Brantley, S.L. (2011) How mineralogy and slope aspect affect *REE* release and fractionation during shale weathering in the Susquehanna/Shale Hills Critical Zone Observatory. *Chemical Geology*, **290**, 31–49.

McLaughlin, J.R.W. (1959) The geochemistry of some kaolinitic clays. *Geochimica et Cosmochimica Acta*, **17**, 11–16.

McLennan S.M. (1989) Rare earth elements in sedimentary rocks: influence of the provenance and sedimentary process. Pp. 169–200 in*: Geochemistry and Mineralogy of Rare Earth Elements* (B.R. Lipin and G.A. McKay, editors). Reviews in Mineralogy, **21**, Mineralogical Society of America, Washington, D.C.

McLennan, S.M., Taylor, S.R., McCulloch, M.T., and Maynard, J.B. (1990) Geochemical and Nd-Sr isotopic composition of deep-sea turbidites: Crustal evolution and plate tectonic associations. *Geochimica et Cosmochimca Acta*, **54**, 2012–2050.

Murray, H.H. (2007) *Applied Clay Mineralogy.* Developments in Clay Science, **2**, Elsevier, Amsterdam, 180 pp.

Murray, H.H. and Keller, W.D. (1993) Kaolin, kaolin and kaolin. Pp. 1–24 in: *Kaolin Genesis and Utilization* (H.H. Murray, W. Bondy, and C. Harvey, editors). Special Publication **1**, The Clay Minerals Society.

Nabawy, B. (2010) Impacts of dolomitization on the petrophysical properties of the Cenomanian El-Halal Formation in its type section, north Sinai, Egypt. *Geophysical Research Abstracts*, **12**, EGU2010-8821.

Nagy, G., Draganits, E., Demeny, A., Panto, G., and Arkai, P. (2002) Genesis and transformations of monazite, florencite and rhabdophane during medium grade metamorphism: examples from the Sopron Hills, Eastern Alps. *Chemical Geology*, **191**, 25–46.

Nance, W.B. and Taylor, S.R. (1976) Rare earth element pattern and crustal evolution: I. Australian post-Archean sedimentary rocks. *Geochimica et Cosmochimica Acta*, **40**, 1539–1551.

Plank, T. and Langmuir, C.H. (1998) The chemical composition of subducting sediment and its consequences for the crust and mantle. *Chemical Geology*, **145**, 325–394.

Prudêncio, M.I., Gouveia, M.A., and Braga, S.M.A. (1995) *REE* distribution in present day and ancient surface environments of basaltic rocks (central Portugal). *Clay Minerals*, **30**, 239–248.

Pruett, R.J. and Murray, H.H. (1993) The mineralogical and geochemical controls that source rocks impose on sedimentary kaolin deposits. Pp. 149–170 in: *Kaolin Genesis and Utilization* (H.H. Murray, W. Bundy, and C. Harvey, editors). Special Publication **1**, The Clay Minerals Society, Indiana, USA.

Pruett, R.J. and Pickering, Jr., S.M. (2006) Kaolin. Pp. 390–427 in: *Industrial Minerals and Rocks* (J. Elzea Kogel, N.C. Trivedi, J.M. Barker, and S.T. Krukowski, editors). Society for Mining, Metallurgy, and Exploration, Inc., Littleton, Colorado, USA.

Rashed, A.F. and Amer, M.N. (1994) Geological and mineralogical studies on some west-central Sinai kaolin deposits and their industrial applications. *Proceedings of the First International Symposium on Industrial Applications of Clays*, Cairo, pp. 306–314.

Saad, N., Zidan, B.I., and Khalil, K.I. (1994) Geochemistry and origin of the manganese deposits in the Um Bogma region, west central Sinai, Egypt. *Journal of African Earth Sciences*, **19**, 109–116.

Schroeder, P.A., Pruett, R.J., and Melear, N.D. (2004) Crystal-chemical changes in an oxidative weathering front in a Georgia kaolin deposit. *Clays and Clay Minerals*, **52**, 211–220.

Shimron, A.S. (1975) Petrogenesis of the Tarr albitite-carbonatite complex, Sinai Peninsula. *Mineralogical Magazine*, **40**, l3–24.

Sousa, D.J.L., Varajão, A.F.D.C., and Yvon, J. (2006) Geochemical evolution of the Capim River kaolin, Northern Brazil. *Journal of Geochemical Exploration*, **88**, 329–331.

Sousa, D.J.L., Varajao, A.F.D.C., Yvon, J., Scheller, T., and Moura, C.A.V. (2007) Ages and possible provenance of the sediments of the Capim River kaolin, northern Brazil. *Journal of South American Earth Sciences*, **24**, 25–33.

Taylor, S.R. and McLennan, S.H. (1985) *The Continental Crust: Its Composition and Evolution*. Blackwell, Oxford, UK, 312 pp.

Turekian, K.K. and Wedepohl, K.H. (1961) Distribution of the elements in some major units of the Earth's crust. *Geological Society of America Bulletin*, **72**, 175–191.

Walley El-Dine, N., Sroor, A., El-Shershaby, A., El-Bahi, S.M., and Ahmed, F. (2004) Radioactivity in local and imported kaolin types used in Egypt. *Applied Radiation and Isotopes*, **60**, 105–109.

Weissbrod, T. (1969) The Paleozoic of Israel and adjacent countries, Part II: The Paleozoic outcrops in Southwestern Sinai and their correlation with those of southern Israel. *Israel Geological Survey Bulletin*, **48**, 32 pp.

Zack, T., Eynatten, H.V., and Kronz, A. (2004) Rutile geochemistry and its potential use in quantitative provenance studies. *Sedimentary Geology*, **171**, 37–58.

(*Received 23 July 2011; revised 8 December 2012; Ms. 594; AE: R.J. Pruett*)